Sascha Winter, BSc

Photoregeneration of cellulose

MASTER'S THESIS

to achieve the university degree of

Diplom-Ingenieur

Master's degree programme: Technical Chemistry

submitted to

Graz University of Technology

Supervisor

Univ.-Prof. Dipl.-Ing. Dr.techn. Franz Stelzer

Mag.rer.nat. Dr.rer.nat. Stefan Spirk

Institute for Chemistry and Technology of Materials
Faculty of Technical Chemistry, Chemical and Process Engineering, Biotechnology

Graz, March 2015

AFFIDAVIT

I declare that I have authored this thesis independently, that I have not used other than the declared sources/resources, and that I have explicitly indicated all material which has been quoted either literally or by content from the sources used. The text document uploaded to TUGRAZonline is identical to the present master‘s thesis dissertation.

Date

Signature

Acknowledgement

Lots of people contributed to this thesis, be it by animated discussion, helpful advice, encouraging words or just simple fun for having a good time at work. Each and every one of these colleagues, friends or relatives deserves my deeply felt appreciation even if it's not possible to mention all of them personally.

First of all, I want to express my overwhelming gratitude to my advisor Dr. Stefan Spirk for giving me the opportunity of working in the field of cellulose research and especially on this overly interesting project. Special thanks to you for your guidance and helpful advice as well as constructive criticism even at hardship. Furthermore, I wish to thank Dr. Thomas Griesser, whose involvement in the project enabled this thesis, for the possibility to work at Montanuniversität Leoben within the Department of Polymer Engineering and Science.

I'd like to thank Dr. Franz Stelzer, head of the Institute of Chemistry and Technology of Materials, for permitting me to do the research work at his institute and the staff of the institute for their assistance and advice.

I address additional thanks to my dear colleagues Heike, Katrin, David and Manuel from our workgroup "AG Spirk" for answering all of my more or less intelligent questions and the ensuing discussions (I'm confident of not having been too distressing …) and to Archim from MU Leoben for helping me out with his knowledge and humor while producing incredible amounts of data.

Michael deserves special thanks for helping me with some nerdy "computer-related" (and many other) problems and even more thanks for staying friends with me for all this time. No one else endured THIS long.

I also want to express my dearest appreciation to my parents and my brother for all the sacrifices they made on my behalf, their never ending support and for never losing faith in me. It's impossible to thank you enough for all you have done for me.

Last but foremost I'd like to thank my better half Christina, who always brings me back down to earth and keeps me focusing with her sweet and unconventional but still unique manner when my thoughts roam in the air. Well, these thoughts are almost exclusively related to you my sunshine. Thank you for prettying my life so much each and every moment.

Motivation & target

Not only its abundancy and environmental sustainability, but most notably the variety of properties are the reason, why cellulose becomes more and more the target of specific research in several fields of science. Based on the numerous advantages and increasing focus on this biopolymer, it is one of the main aims to make it accessible to even more fields of application. Transforming native, fibrillar cellulose into amorphous thin films, that facilitate various applications is one important step to use cellulose more efficiently. This accomplishment already applies to the preparation of organic thin-film transistors (OTFT), simulation of bulk material or immobilisation and adsorption studies of other biomolecules. For achieving even better results within the named fields, it is inevitable to work on improvements in the patterning of cellulose.
Instead of using methods that are unprecise, laborious or expensive, photoacid generators (PAG) offer a promising perspective to circumvent these disadvantages. PAGs have already proven themselves in e.g. resist systems and polymerisation initiation, what suggests their utilisation in the given task.

Abstract

Knowledge of cellulose is increasing ever since its discovery, thus cellulose is more and more in the focus of interest regarding its abundancy, sustainability and outstanding material properties. Within the scope of this work a novel technique of regenerating cellulose thin films by means of photolithographic methods for the fabrication of patterned surfaces is investigated. In preparation for future research concerning the achievement of higher lateral resolutions, five photoacid generators are examined in terms of their efficiency and the properties of resulting cellulose films. It will be shown, that the acid generating capabilities of tested photoacid generators differ strongly from each other and they are partially affected by extension of the chromophore through substitution, while topography and thickness of the obtained layers exhibit similarity.

Since all experiments regarding the preparation and development of cellulose thin films are carried out in chloroform, it is sought to create new substrates to accomplish an exchange of solvent to “eco-friendly” alternatives. For this reason a straightforward method for the production of trimethylsilyl cellulose with adjusted degrees of substitution is presented, in order to use ethanol or ethyl acetate as solvents.

Kurzfassung

Seit ihrer Entdeckung rückt Cellulose mehr und mehr ins Zentrum des Interesses, bedingt durch das steigende Wissen über Qualitäten, wie zum Beispiel ihre Unerschöpflichkeit, Nachhaltigkeit und die herausragenden Materialeigenschaften. Im Rahmen dieser Arbeit wird eine neuartige Methode zur Regeneration von Cellulose-Dünnfilmen untersucht, die sich der Prinzipien der Photolithographie bedient und die Herstellung strukturierter Oberflächen zum Ziel hat. So werden fünf Photosäuregeneratoren auf deren Effizienz und die Eigenschaften der resultierenden Cellulose-Filme untersucht, um zukünftige Forschung bezüglich des Erreichens höherer räumlicher Auflösung bei der Strukturierung zu unterstützen. Erhebliche Unterschiede in der Fähigkeit der getesteten Photosäuregeneratoren Säure freizusetzen, sowie deren Abhängigkeit von Erweiterungen des Chromophors mit verschiedenen Substituenten, werden aufgezeigt, wobei jedoch Oberflächenbeschaffenheit und Schichtdicke der resultierenden Cellulose-Filme große Ähnlichkeit aufweisen.

Des Weiteren wird versucht das, für die Herstellung und Entwicklung der Cellulose-Dünnfilme benötigte, Chloroform durch nachhaltigere und umweltfreundlichere Alternativen wie zum Beispiel Ethanol oder Essigsäureethylester zu ersetzen. Zu diesem Zweck wird mit Hilfe einer einfachen Methode Trimethylsilylcellulose hergestellt, deren Substitutionsgrad – in Bezug auf Silylgruppen – einstellbar ist.

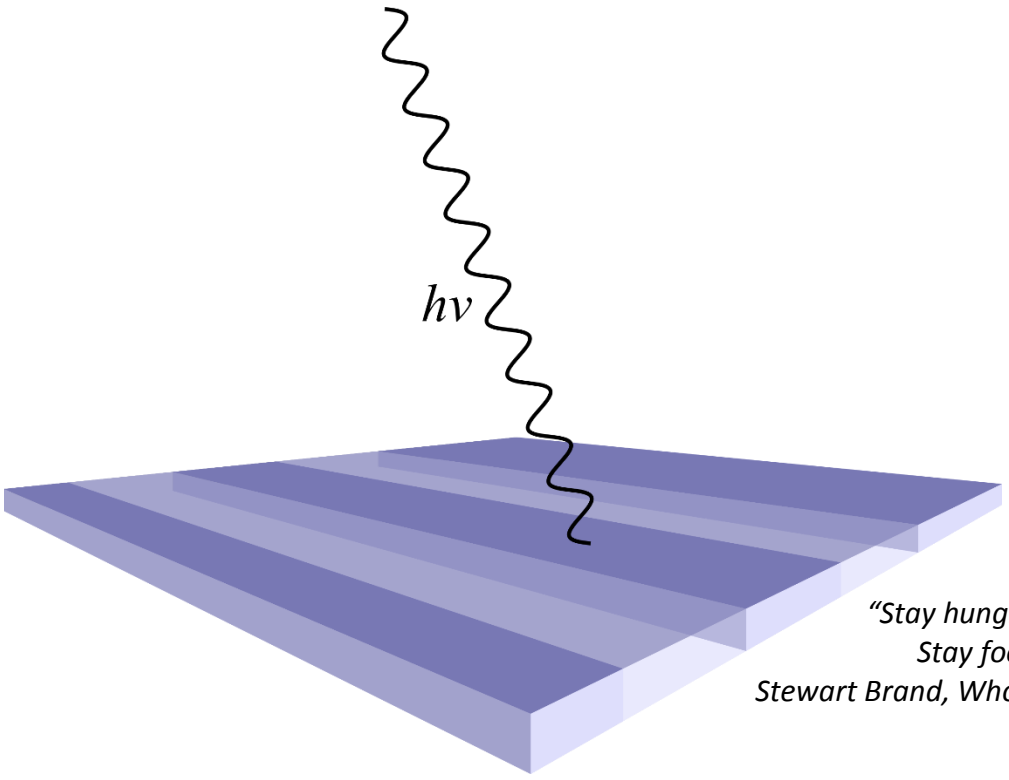

"Stay hungry.
Stay foolish."
Stewart Brand, Whole Earth Catalog

Table of contents

Introduction

Besides other natural polymers such as pectin, lignin and hemicellulose, cellulose represents the most important structural constituent of primary and secondary plant cell walls.[1, 2] Single strands consist of hundreds to thousands of β(1→4) linked D-glucose units, which form fibrils embedded in a matrix of aforementioned components (see *Figure 1*).[3]

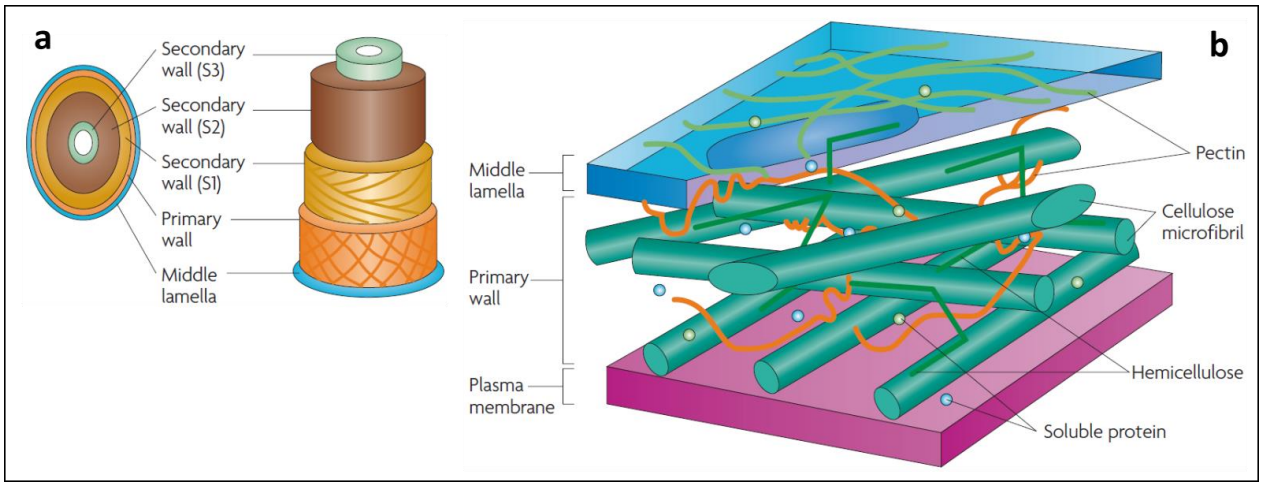

Figure 1. Schematic structure of plant cell walls, a) main parts of a plant cell wall, b) constituents present in the primary wall. from M. B. Sticklen, Nature Reviews Genetics ***2008**, 9, 433-443*

Estimating an annual amount of 10^{11}-10^{12} tons of polysaccharide, cellulose represents the most abundant biopolymer in the world.[1] It has been used in the form of paper, cotton or wood, as energy source, building material or textiles for thousands of years.[4] Its breakthrough as a chemical raw material took place in 1838, when cellulose was first discovered as remains of plant tissue after acidic treatment by the French chemist Anselme Payen.[4, 5] Thereafter, scientists endeavoured to reveal the structure of cellulose - which could not be achieved until Staudinger's pioneering findings concerning polymers in 1920[6] (see *Figure 2*) - and to find new possible fields of application. Some of the milestones that marked the early stages of cellulose chemistry were the synthesis of cellulose nitrate by Schönbein in 1846[7], the discovery of Schweizer's reagent $[Cu(NH_3)_4](OH)_2$ - what was mentioned being the first cellulose solvent - in 1857[8] and the synthesis of cellulose acetate by Schützenberger in 1865.[9] First industrial success was achieved in 1870 when celluloid - the first thermoplastic polymer - was produced by the Hyatt

Manufacturing Company based on cellulose nitrate with camphor as plasticiser.[4] Due to safety issues and difficult and expensive production celluloid was superseded by cellulose triacetate.

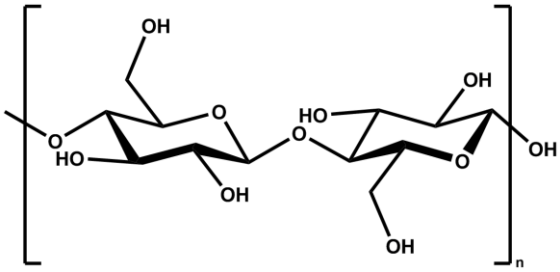

Figure 2. Repeating unit of cellulose; cellobiose

Extended knowledge of the material led to the production of synthetic filaments on the basis of wood cellulose by the help of regeneration processes. The first example thereof is the utilisation of aforementioned Schweizer's reagent followed by the viscose process[10]; the most important industrial method for the production of regenerated cellulose fibres up to the present day. All processes have to deal with a serious drawback in terms of homogenous reactions: cellulose is poorly soluble in common organic solvents and water. Two possibilities for bypassing this problem are subject to continuous research. These comprise the use of complex solvents or solvent mixtures (e.g. *N,N*-dimethylacetamide (DMAc)/LiCl, *N*-methylmorpholine *N*-oxide (NMMO)) and the synthesis of cellulose derivatives featuring solubility in certain solvents.

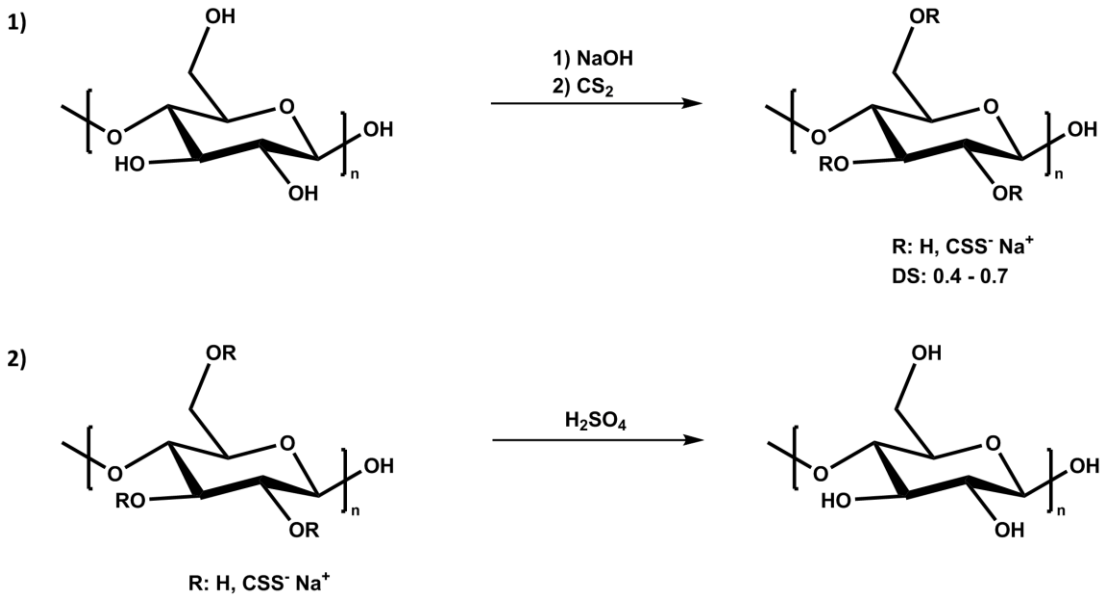

Figure 3. Overview of the basic chemical steps of the viscose process; step 1: preparation of cellulose xanthate, step 2: regeneration of cellulose

The viscose process - invented by Cross, Bevan and Beadle in 1892 - uses the second path; by reacting cellulose with sodium hydroxide and carbon disulphide, cellulose xanthate with an average degree of substitution of 0.4 to 0.7 is produced (see *Figure 3*). The newly created cellulose derivative is now soluble in aqueous NaOH. After several steps including filtration and degassing of the solution, regenerated cellulose fibres are precipitated in an acid bath via wet spinning.[11] This precipitation process in combination with the reconversion to cellulose, whether from solvents like *N*-methylmorpholine *N*-oxide or ionic liquids for instance, is called regeneration of cellulose. The industrial application of the xanthate pathway to produce regenerated cellulose led to the development of several new products like Cellophane[12] - a transparent film of cellulose primarily used as packaging material - and Visil rayon[13] - flame-retardant cellulose fibres containing polysilicic acid. Further research regarding environmental aspects resulted in the invention of new methods like the Lyocell process[4] or the silyl technique[14, 15], both strongly influenced by the Lenzing AG.

While the Lyocell process uses NMMO/water as solvent for cellulose, the silyl technique utilises organosilicon compounds to derivatise cellulose creating new materials with varying solubility depending on the degree of substitution. Despite promising properties of the products the method was not used for industrial purposes so far.[16, 17] In turn, the interest in organosilyl celluloses rose, when scientists took notice of the outstanding properties, in terms of producing ultrathin cellulose films.[18] Initially trimethylsilyl cellulose - already known in the late 1940s[19] - was used to create monolayers, which were subjected to HCl vapour, converting TMSC to cellulose in situ.[20] The method of choice to obtain monolayers of cellulose or cellulose derivatives is the Langmuir-Blodgett technique, which works well with hairy-rod molecules. The elementary procedure for generation of thin films involves the application of the layer material on the liquid's surface, followed by deposition onto a solid substrate by immersion into or emersion from the liquid, while the molecules located at the air-liquid interface are subjected to constant lateral pressure. However, the main advantages of the LB technique - the creation of highly ordered monolayers with distinct thickness - come at the cost of being expensive and laborious.[18, 21]

The introduction of the spin coating technique to prepare thin films[22, 23] allowed for developing new fields of application, since this method enables fast and reproducible preparation of highly

amorphous cellulose films. These applications comprise simulation of bulk material[24], adsorption studies for different biomolecules and their immobilisation[25, 26] and utilisation of dielectric properties in organic thin-film transistors (OTFT)[27] with the latter requiring efficient production methods in terms of patterning techniques.

Here it has to be mentioned, that the development of potent methods for lateral and three-dimensional structuring of thin films is crucial, in order to exploit some of the numerous advantages of cellulose. These comprise biocompatibility and low toxicity combined with hydrophilicity and low fouling properties.[4, 25, 28] Furthermore cellulose provides a convenient and straightforward method to cast films in the order of 10 to 50 nm by spin coating[22, 23], which offer a high surface area and a stable environment for the adsorption of biomolecules.[29-32] In combination with the fact, that cellulose is an insulator, all these qualities encourage the utilisation of cellulose for a broad variety of applications as for example microfluidic systems, microarrays and biochips[33], as well as aforementioned OTFTs. These fields of application have in common, that they are susceptible to miniaturisation in terms of cost reduction (decreased material and power consumption), flexibility (facilitated transport) and performance (more components per chip).[34, 35] Therefore, it is - as already mentioned - necessary to develop new patterning methods that allow for an efficient size reduction.

Current methods for this purpose involve enzymatic digestion, soft lithography, deep UV lithography and combinations thereof, each of them having advantages and disadvantages. Referring to the enzymatic pathway, basically it is a simple but laborious technique inasmuch as relying on preparatory work. These preparations can be either local regeneration of cellulose, with the unregenerated area not being digested, or the application of microstructured elastomeric moulds to form microchannels between cellulose film and mould, which in turn requires the fabrication of micromilled templates serving as master for the creation of said moulds. This accounts for the method having lesser drawbacks regarding precision, which is true for soft lithography as well. Differences between the latter and enzymatic digestion are limited to the needed effort, since the lithographic technique uses the same moulds as stamps or microchannels, transferring biomolecules to a cellulose surface without prior structuring, leading to similar lateral resolutions. Another method uses masks to partially cover a film of TMSC, regenerating only the parts exposed to HCl vapour. [25, 26] Deep UV lithography on the other hand

is characterised by yielding very small feature sizes due to the small wavelengths used. The downsides include a high energy input and limitations in its usage in terms of materials not withstanding the exposure to highly energetic UV-light (e.g. OTFT). Regarding the behaviour of cellulose upon irradiation with UV-light, it has been found, that wavelengths below 290 nm may lead to cleavage of glycosidic bonds. Further investigations on the photodegradation of cellulose revealed elimination processes yielding H_2, CO_2 and CO when exposed to UV-light with 253.7 nm, while lower wavelengths (e.g. extreme UV) resulted in scission of the anhydroglucose unit (AGU).[36, 37] Regarding aforementioned characteristics, another method is needed for making the patterning process technically valuable and therefore attractive for industrial application.

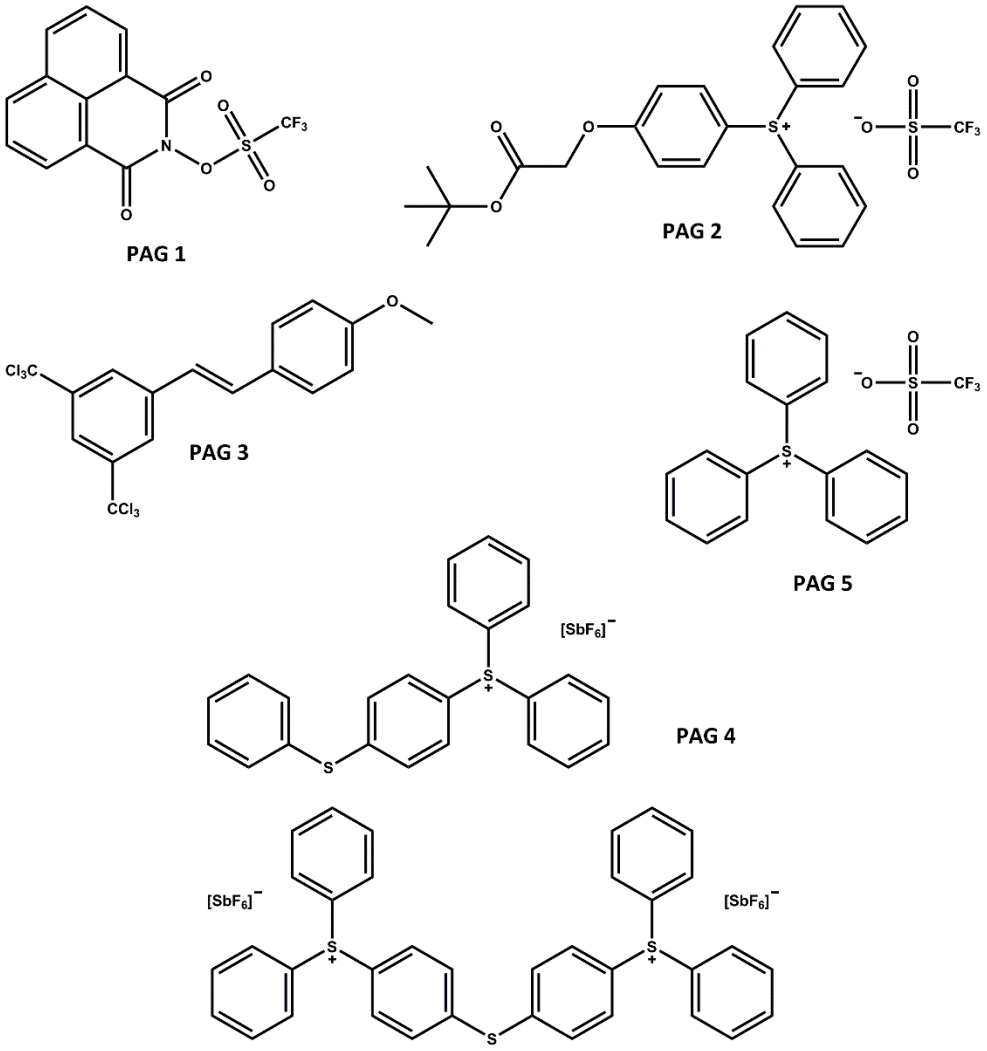

Figure 4. Overview of the chemical structures of photoacid generators used within the scope of this thesis

In this work a novel method based on the photoinduced alteration of the substrates solubility by elimination of the acid-labile organosilyl protecting groups is used. The fundamentals of this technique were first proposed in the early 1980s, when it was attempted to amplify resist systems chemically.[38] The compounds required for an amplification are photoacid generators (PAG); molecules with chromophoric areas, which are able to produce Brønsted acid upon UV irradiation. Despite the knowledge of the compounds' existence had been noted almost a century ago, their present fields of application involving cross-linking and degradation of polymers and initiation of polymerisations were discovered much later.[39] According to literature, the effect of photoacid generators on other cellulose derivatives (e.g. cellulose acetate[40, 41]) has already been investigated, with results suggesting a possible viability of the method regarding systems based on other polysaccharides like chitin or chitosan.

PAGs can be divided into two main classes, i.e. ionic and non-ionic photoacid generators. Typically, non-ionic systems involve *o*-nitrobenzyl esters of carboxylic acids, *N*-hydroxy-naphthalimide sulphonates, triarylphosphate derivatives and aryl halides generating carboxylic acids, sulphonic acids, phosphoric acids and hydrogen halides, respectively.[42] While it is advantageous for these PAGs being soluble in a large number of possible solvents, their main disadvantage is a lesser thermal stability compared to ionic photoacid generators, although these properties may be altered by means of different substitution. As mentioned before, the second group of PAGs are ionic compounds involving onium salts (e.g. aryldiazonium, diarylhalonium, triarylsulphonium and triarylphosphonium salts) including anionic metal halides such as BF_4^-, SbF_6^-, AsF_6^- and PF_6^-. In contrast to non-ionic species, the thermal stability of photoacid generator salts is superior, while poor solubility in common organic solvents represents their main disadvantage. However, the aforementioned possibilities of changing the properties in terms of structural modification applies to ionic PAGs as well, comprising the alteration of absorption characteristics.[39]

When PAGs are subjected to UV irradiation of a certain wavelength range, they undergo a specific decomposition process, associated to the type of photoacid generator. Since the degradation mechanisms of the PAGs used in this thesis are well studied, they are presented in the following. The five compounds examined are namely *N*-hydroxynaphthalimide triflate (PAG **1**), *Boc*-methoxyphenyldiphenylsulphonium triflate (PAG **2**), 2-(4-Methoxystyryl)-4,6-bis-(trichloro-

methyl)-1,3,5-triazine (PAG **3**), triarylsulphonium hexafluoroantimonate salts (PAG **4**) and triphenylsulphonium triflate (PAG **5**) three of them being ionic photoacid generators of the same kind as can be seen in *Figure 4*.

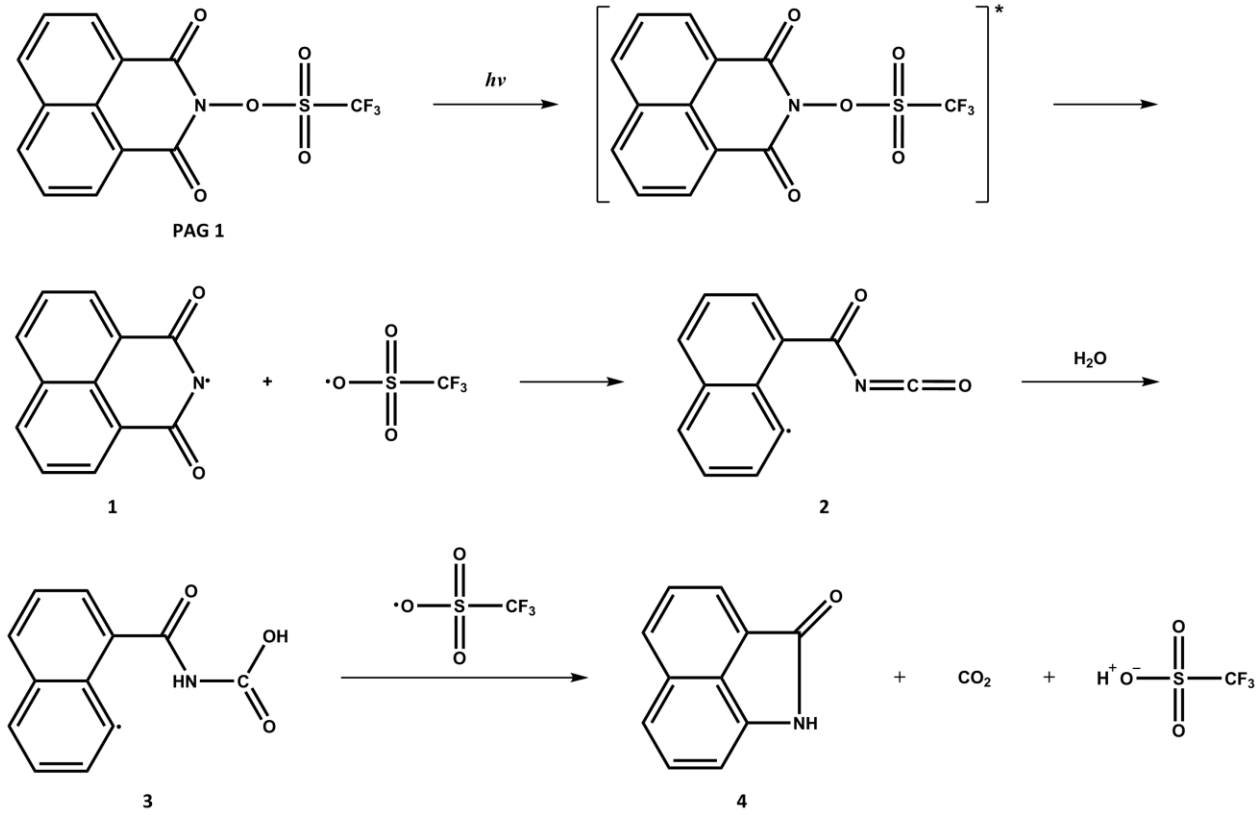

Figure 5. Mechanism of dissociation upon UV-light irradiation of N-hydroxynaphthalimide triflate

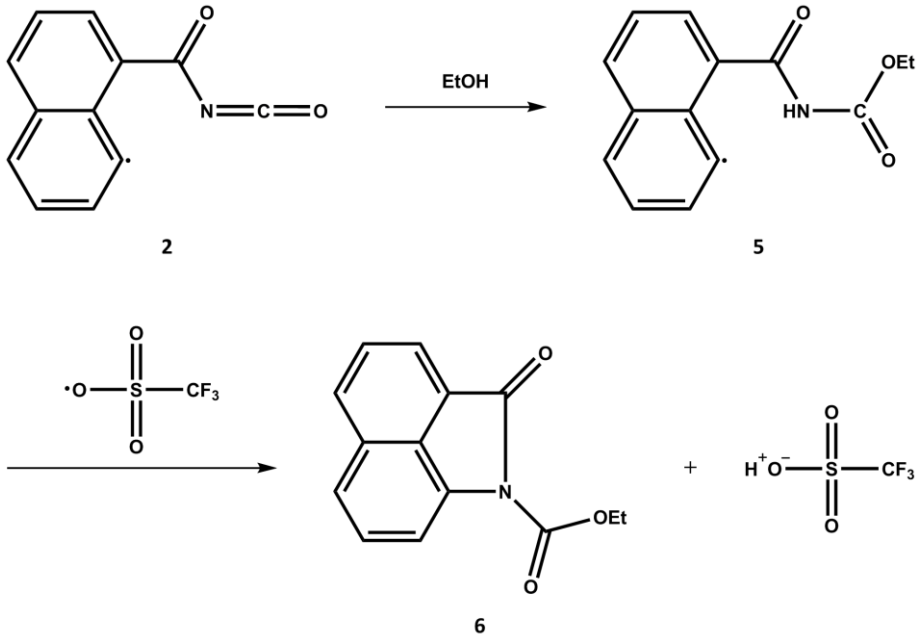

*Figure 6. Alternative decomposition pathway of PAG **1**, due to change of solvent to EtOH*

Starting with PAG **1**, its reaction pathway upon irradiation is shown in *Figure 5*. As pointed out, the first step involves the light-induced activation of the molecule to the excited state, which happens to the other photoacid generators in the exact same way. In the next steps homolytic cleavage of the N-O-bond occurs, followed by an intramolecular rearrangement reaction yielding isocyanate **2**. After nucleophilic attack of water and the removal of hydrogen by tosyl radical, carbon dioxide is eliminated and benzo[*cd*]indol-2(1*H*)-one **4** is formed. Investigations revealed, that several factors have to be considered, in order to maximise the quantum yield of photoacid generation. In the case of PAG **1**, a hydrogen source is needed, either from the solvent, substrate or another compound chosen specifically for this task. In terms of solvents, it has been found that increasing polarity reduces fluorescence and intersystem crossing quantum yields, which are assumed to be competitive pathways to acid generation. Another effect that can be attained by choice of solvent is a modified reaction path meaning a different product is obtained (e.g. ethanol, see *Figure 6*). Furthermore the energetic characteristics have been investigated.

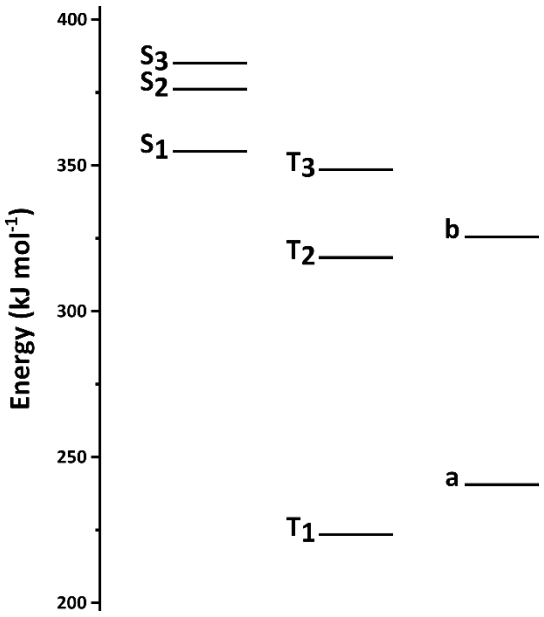

*Figure 7. Calculated energy levels of singlet excited states (S), triplet excited states (T), heterolytic (b) and homolytic cleavage (a) for PAG **1** upon irradiation*

Phosphorescence and fluorescence measurements and calculations resulted in a diagram of singlet and triplet, as well as cleavage product energy levels, which is shown in *Figure 7*. It can be seen that homolytic cleavage of *N*-hydroxynaphthalimide triflate from the lowest triplet state is an endergonic process, while singlet state homolysis is clearly exergonic. Since fluorescence

emission spectra recorded during photolysis exhibit an isoemissive point, it has been stated that photoacid generation should proceed from the excited singlet state. In addition the dipole moment of the singlet excited state was calculated and compared to the dipole moment of the ground state. The results revealed only a minor change which means the excited state has a weak polar character and therefore heterolytic cleavage should not be favoured.[43-45]

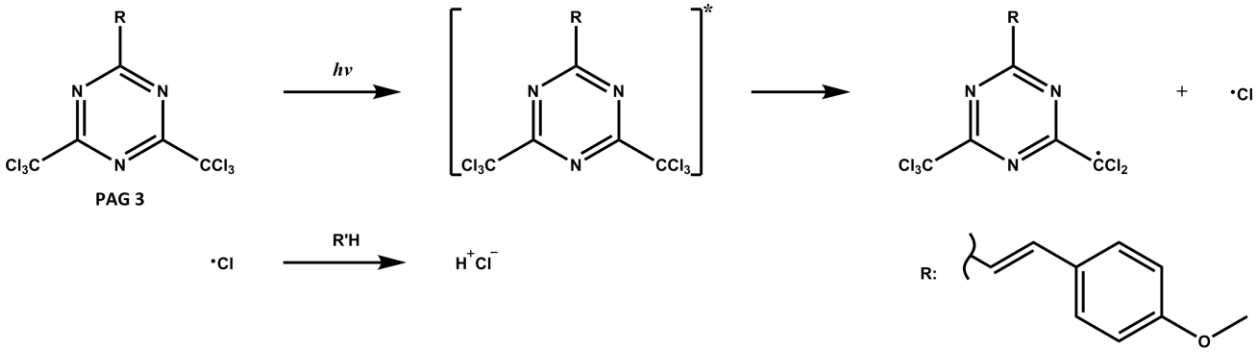

Figure 8. Mechanism of decomposition upon UV-light irradiation of 2-(4-methoxystyryl)-4,6-bis(trichloromethyl)-1,3,5-triazine

Examining PAG **3**, its decomposition pathway - as proposed in literature - can be seen in *Figure 8*. In contrast to PAG **1** there are no rearrangement reactions involved; the chlorine radicals generate acid directly via abstraction of hydrogen from substrate, solvent or the like. PAG **3** represents a compound that was altered by chromophore substitution, in order to extend the wavelength range of response as well as to improve the spectral sensitivity and absorption characteristics. It was found, that the compound exhibits a lack of fluorescence and phosphorescence, latter denoting an inefficient depletion of the excited singlet state by intersystem crossing. Additionally, laser flash photolysis experiments demonstrated rather strong differences between PAG **3** and its parent compound 2-methyl-4,6-bis(trichloromethyl)-1,3,5-triazine, which include a strong ground state bleaching and therefore interferences in detection of an already low amount of chlorine, causing the utilisation of titration methods to determine acid formation efficiency. Energetic reasons for the observed, low quantum yield are not fully understood due to a lack of photophysical data and suitable methods for observation of singlet and triplet states. It is supposed, that a combination of low excitation energies of S_1 and T_1 states as well as more efficient deactivation processes thereof are the main reasons for the poor performance.[46-48]

The last group of investigated photoacid generators are the ionic sulphonium salts. The pathway of photoinduced cleavage for the tested compounds is shown in *Figure 9*. The product distribution depicted in the same figure represents the summary of possible photoproducts due to its dependence on the reaction conditions and sulphonium cations used. Photodissociation of PAG **5** - the parent compound - yields diphenyl sulphide **8**, biphenyl **11** and (phenylthio)biphenyls **7** with the major products being *o*-(phenylthio)biphenyl and diphenyl sulphide. The main percentage of recombination photoproducts is considered to originate from in-cage fragmentation-recombination reactions or intra-molecular rearrangement. Since the photoproducts formed still hold their chromophoric character, the possibility of "inner-filter-effects" and potential secondary photolysis arises, resulting in an altered product distribution (e.g. biphenyl formed from (phenylthio)biphenyl). The substitution of one or more phenyl rings leads to different fragmentation pathways. It has been found, that the preferentially cleaved aryl fragment contained the electron donating group and therefore the major sulphide formed carried the electron withdrawing group. While the amount of acid generated correlates well with total product formation, the quantity differs with varying substitution.

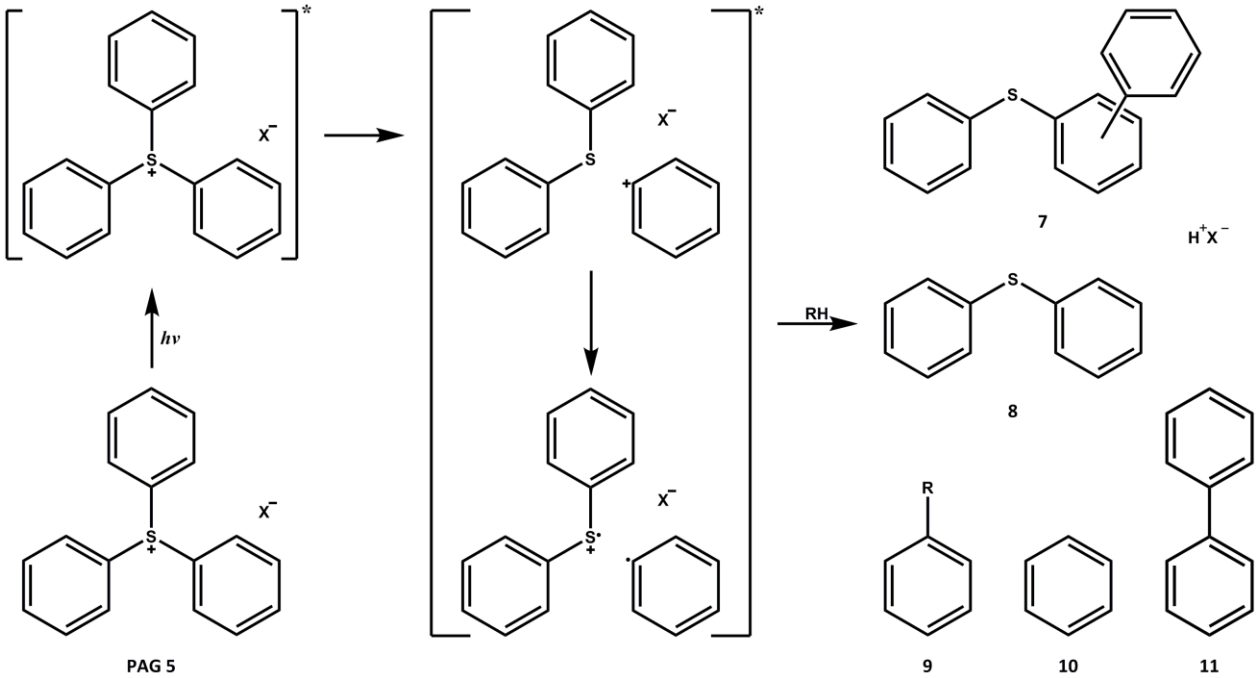

Figure 9. Mechanism of decomposition upon UV-light irradiation of triarylsulphonium salt photoacid generator

Alkyl ether moieties lower the efficiency (e.g. (4-methoxyphenyl)diphenylsulphonium: 64% efficiency), whereas a phenylthio moiety provides an increase of 12% compared to triphenyl-sulphonium, even though the absorption maximum of [4-(phenylthio)phenyl]diphenyl-sulphonium is shifted to lower energy than (4-methoxyphenyl)diphenylsulphonium. Compared to other sulphonium salt photoacid generators, the photochemistry of [4-(phenylthio)phenyl]-diphenylsulphonium is unusual - compared to sulphonium salts containing other electron-donating moieties (e.g. methoxyphenyl groups) - but has been explained by singlet state stabilisation and increased intersystem crossing. It has been stated, that the major path of decomposition is heterolysis while homolysis represents a minor pathway, which is converse in case of the phenylthio-compound. Furthermore, the photodissociation of the latter proceeds through the triplet state as indicated above. Inferring from the facts mentioned sulphonium salt photoacid generators appear more efficient if dissociated by homolysis.[48-55]

Experimental

Materials

Microcrystalline cellulose (MCC, Sigmacell Cellulose Type 20), triethylamine (≥99%), *N,N*-dimethylacetamide (DMAc, anhydrous, 99.8%), lithium chloride (99%, anhydrous), potassium hydrogen phosphate (≥98%, anhydrous), potassium dihydrogen phosphate (≥99%, anhydrous), ethanol (≥99.8%), *N*-hydroxynaphthalimide triflate (≥99%, PAG **1**), *Boc*-methoxyphenyldiphenyl-sulphonium triflate (PAG **2**), 2-(4-Methoxystyryl)-4,6-bis(trichloromethyl)-1,3,5-triazine (98%, PAG **3**), triaryl-sulphonium hexafluoroantimonate salts (50 %(w/w) in propylene carbonate, PAG **4**), triphenyl-sulphonium triflate (PAG **5**) and trimethylsilyl chloride (TMSCl, ≥99%, Fluka) were purchased from Sigma-Aldrich, Steinheim, Germany. Trimethylsilyl cellulose with a degree of substitution of 2.8 was provided by TITK Rudolstadt, Germany and chloroform (J.T.Baker) was obtained from VWR International GmbH, Vienna, Austria. All chemicals were used without further purification except for MCC and LiCl, which were dried for 12 hours at 100°C under reduced pressure.

Silylation of cellulose

In a typical procedure a 100 mL three-necked flask equipped with thermometer, reflux condenser, gas inlet and outlet was purged with nitrogen before adding 1.00 g (6.17 mmol AGU) of dried cellulose. The cellulose was suspended in 30 mL (0.32 mol) of DMAc and stirred for 2 hours at 150°C. The mixture was left to cool to 80°C and 1.80 g (42.5 mmol) LiCl were added. Stirring continued without heating until the polymer completely dissolved.

Afterwards, 1.76 g (17.4 mmol) of triethylamine were added under vigorous stirring. After dissolution of the triethylamine occurred, a defined amount of TMSCl was added and stirring was continued for 24 hours. The mixture was poured into 500 mL of cooled phosphate buffer containing 3.57 g (20.5 mmol) of K_2HPO_4 and 1.77 g (13.0 mmol) KH_2PO_4. The white, solid product was filtered off and washed 5 times with water and additionally 3 times with ethanol, in case the

expected DS_{Si} was higher than 1.5. The obtained TMSC was dried for 5 hours in a vacuum oven at 100°C prior to dissolution experiments, which were conducted in different ways for testing purposes. Small amounts of a sample were put into three glass vial and solvent was added. The vials were closed and subjected to vigorous shaking, heating and a combination of these methods, respectively. In order to examine how much of TMSC actually dissolved, the solid residues were filtered off and the solvent was then removed from the filtrate by vaporisation. All experiments were repeated with using precipitation in cooled water as detection method instead of drying.

Photoregeneration of cellulose

400 mg of commercial TMSC were added to a glass vial with screw top and magnetic stirrer. After addition of 20 mL of chloroform the mixture was stirred for 4 hours. The obtained solution was successively filtered through 1-2 µm and 0.45 µm syringe filters. The effective concentration of the achieved solution was determined gravimetrically and adjusted to 10 mg/mL before dissolving a distinct amount of each photoacid generator (PAG) in separate TMSC solutions. The concentrations of PAGs in the resulting solutions were 1 %(w/w), 2 %(w/w), 5 %(w/w), 10 %(w/w) and 15 %(w/w), respectively.

Each solution was spin coated on CaF_2 platelets, with the substrates being mounted in petri dishes (Ø = 50 mm) to saturate the surrounding atmosphere with solvent, after which the thin films were illuminated for 16 minutes in total. A schematic overview of the steps included in the fabrication of regenerated thin films is given in *Figure 10*. Irradiation experiments were carried out with a medium pressure Hg-lamp (100 W, 66990, Newport). In order to follow the progressing regeneration, IR measurements were conducted repeatedly after specific time intervals within the overall illumination time. The same procedure was used for preparation of AFM samples with silicon wafers (10 x 10 mm^2) instead of CaF_2 platelets. Additionally, these specimens were developed after the measurement by deposition of the wafers in chloroform for 10 minutes at room temperature. For film deposition at increased humidity, a container filled with water was placed into the spinning chamber and allowed to equilibrate for 30 minutes before spin coating. Prior to use all substrates applied to the procedures described in this section were rinsed

thoroughly with water and acetone and cleaned with a polymer cleaning solution (First Contact, Photonic Cleaning Technology LLC, Platteville, USA).

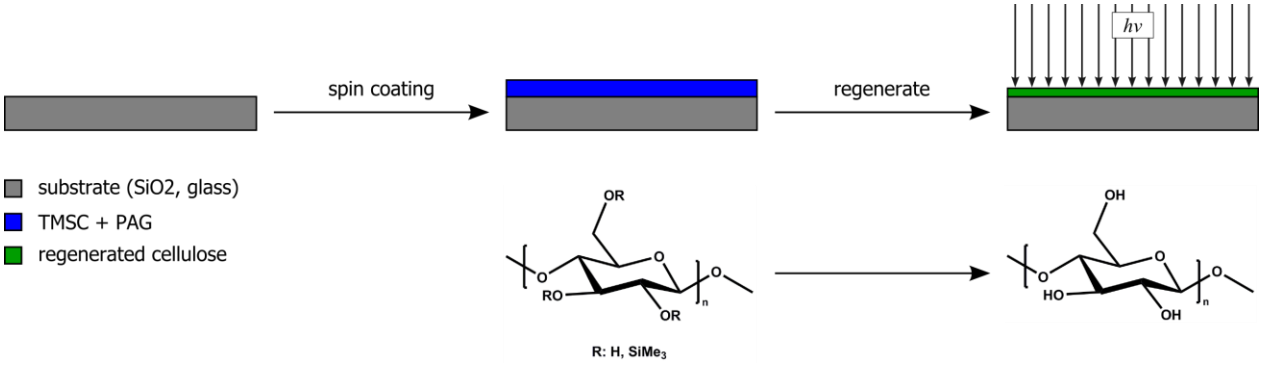

Figure 10. Schematic workflow overview of steps involved in the fabrication of regenerated cellulose thin films based on spin coating a mixture of TMSC and PAG

Measurement

ATR FTIR spectra were acquired with a Bruker ALPHA spectrometer (spectral range: 4000 - 400 cm^{-1}, resolution: 1 cm^{-1}), whereas transmission measurements were conducted on a Bruker VERTEX 80 spectrometer with usage of CaF_2 platelets as substrates for the thin films (spectral range: 4000 - 850 cm^{-1}, resolution: 1 cm^{-1}). Data evaluation was performed by using the OPUS software package (Bruker, Corporation, USA). In order to compare the values of silicon concentration in the regenerated films the peak height of the Si-C signal at ~1250 cm^{-1} was calculated and converted to relative percentages.

UV-Vis absorption was measured on a Varian Cary 50 UV-Vis spectrophotometer using quartz cuvettes with a light path length of 10 mm and chloroform as solvent. The concentration of sample solutions was adjusted to 10 µg/mL regarding evaluability in terms of the Beer-Lambert law. For enabling comparability of the photoacid generator efficiencies at given conditions the respective absorption spectra $f(A_\lambda)$ were used as weight functions, which were applied to the emission spectrum $f(E_{e\lambda})$ of the medium pressure mercury lamp to receive the specific spectral irradiance $E_{e\lambda}^{spec}$ of the tested photoacid generators.

Equation 1.

$$E_{e\lambda}^{spec} = \int \big(f(E_{e\lambda}) * f(A_\lambda)\big) d\lambda$$

The obtained functions were integrated to acquire the specific irradiance E_e^{spec} incident on the surface of the samples. According equations for this task are shown in the following:

Equation 2. $$E_e^{spec} = \int f\left(E_{e\lambda}^{spec}\right) d\lambda$$

In the next step the irradiation time is taken into account to obtain the radiant exposure H_e^{spec}, which is described in Formula 3.

Equation 3. $$H_e^{spec} = E_e^{spec} * t$$

Static contact angles were acquired with a Krüss DSA100 Drop Shape Analyzer with water using a drop volume of 2.0 µl. This measurement served as an additional method to determine the degree of conversion over the course of the experiment, since hydrophilicity increases with a decreasing amount of TMS groups.

AFM images were recorded with a Nanosurf Easyscan 2 FlexAFM in tapping mode using TAP190AL-G silicon probes (resonance frequency: 190 kHz, force constant: 48 N/m). AFM data was evaluated with Gwyddion and WSxM SPM data analysis software[56]; images were equalised by cutting off outliers. For thickness measurements, the samples were scratched with the tip of plastic tweezers applying moderate pressure followed by recording a 20 x 20 µm^2 micrograph with an amplitude of 200 mV and 0.5 seconds run time per line. The mean thickness for each sample was acquired by computing average values of 5 height profiles created by means of the mentioned software. Roughness was determined on the basis of a 5 x 5 µm^2 image (amplitude: 120 mV, run time per line: 0.7 s).

Results & Discussion

Synthesis of trimethylsilyl cellulose

In order to shift the process of regenerating cellulose with the assistance of photoacid generators to economically sound conditions, it is necessary to prepare trimethylsilyl cellulose soluble in "eco-friendly" solvents, such as ethanol or ethyl acetate. The chosen approach employed in this work consists of altering the solubility of TMSC via changes in the degree of substitution.

As already mentioned, the silylation of cellulose - being a heterogeneous process conducted in anhydrous pyridine with trimethylsilyl chloride - was discovered in the late 1940s.[19] In order to increase the maximum attainable degree of substitution, it was necessary to create homogeneous conditions, since it was not possible to achieve full functionalisation, due to the inaccessibility of some hydroxyl groups, which are responsible for the complex supramolecular structure of cellulose induced by strong hydrogen bonding. The most common solvent is a mixture of *N,N*-dimethylacetamide and lithium chloride, which was studied and optimised for a long period of time[57-60]; other more recent examples for homogeneous systems comprise dimethyl sulphoxide/tetrabutylammonium fluoride[61, 62] and ionic liquids[63, 64], both of these being convenient and straightforward, but expensive as well. Since the target of this work is the adjustment of DS_{Si} to obtain TMSC soluble in "eco-friendly" solvents, heterogeneous systems are also qualified for this task.[65] However, the inhomogeneous distribution of silyl groups and laboriousness in terms of processing are major disadvantages, that cannot be overlooked.

Due consideration should be given to the fact, that cellulose needs to be activated prior to dissolution, with several possibilities being available for this purpose; preferable methods are for example heating and solvent exchange. While there are even more methods for activation of cellulose, most of them either derivatise the substrate (e.g. ethylisocyanate) or pose a risk of substrate degradation (e.g. alkaline pre-treatment).[60] Hence, latter approaches are avoided and it was decided to use thermal activation as the treatment of choice, since solvent exchange represents a very laborious and time-consuming alternative. It still has to be pointed out, that

processing of cellulose at elevated temperatures causes degradation as well, which can be observed by discolouration of the reaction mixture.

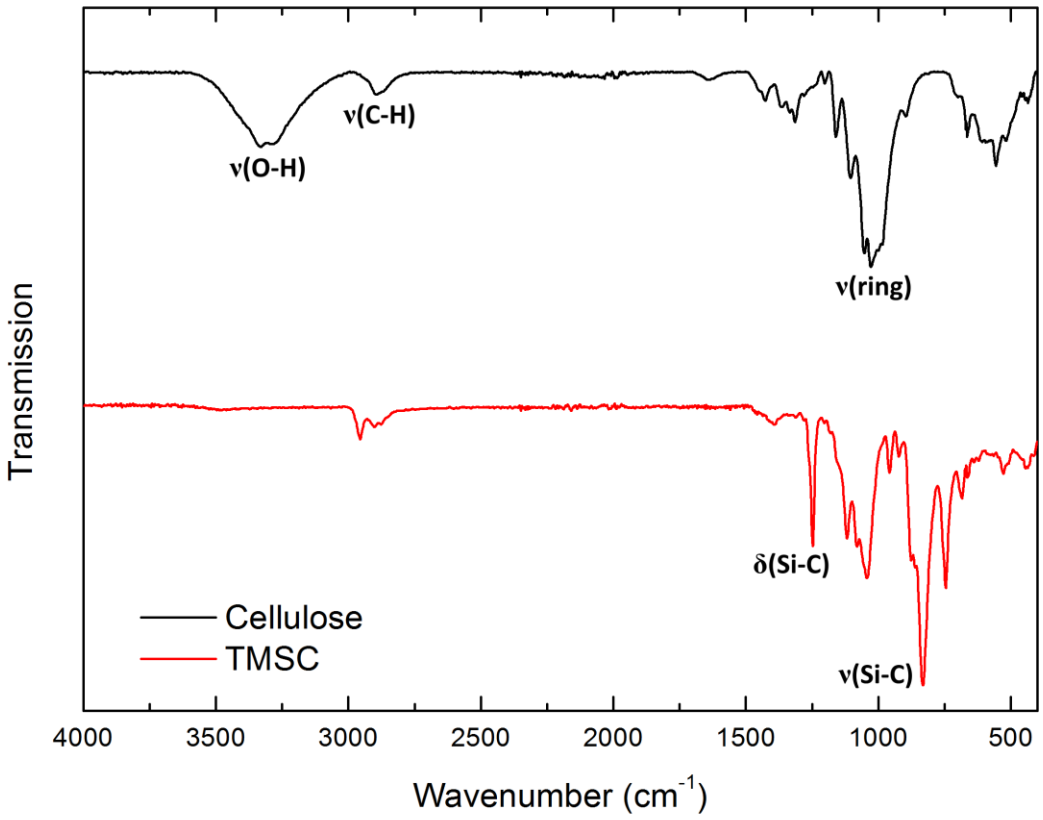

Figure 11. ATR FTIR spectra of Sigmacell cellulose powder and commercial TMSC powder (DS_{Si} 2.8)

In the first step, ATR FTIR spectra of Sigmacell cellulose and commercial trimethylsilyl cellulose were recorded (see *Figure 11*). The spectrum of cellulose shows the predicted, broad band of O-H stretching vibrations between 3000 and 3600 cm^{-1}, whereas the spectrum of TMSC only exhibits a barely noticeable displacement of the baseline in the mentioned area. Other signals associated with vibrations of the O-H groups as for instance bands at 1334 or 1202 cm^{-1} disappear as well. In the region of C-H stretching vibrations two new signals arise at 2955 and 2877 cm^{-1}, respectively. These two bands can be related to asymmetric and symmetric C-H stretching vibrations of the methyl groups attached to silicon which are also accounting for the C-H bending vibration signal at 746 cm^{-1}. Further the contributions of the ring system exhibit alteration, which can be explained by changes in ring conformation due to substitution with bulky trimethylsilyl groups. Other observed variations between the shown spectra are directly related to the TMS groups.

Bending and stretching vibrations of Si-C can be observed at 1248 and 832 cm^{-1}. All observations are in agreement with previous results and summarized in *Table 1*.[23, 66-68]

Table 1. Summary of main IR bands observed in the spectrum of commercial TMSC with an average DS_{Si} of 2.8

Frequency / cm^{-1}	Interpretation
3594-3390	OH stretching
2956	CH_3 asymmetric stretching
2902 2876	CH symmetric stretching
1393	CH_2 in-plane bending
1248	Si-CH_3 in-plane bending
1118	Si-O-C asymmetric stretching
1080	OH bending
1043	C-O stretching
958.3	Si-O-C stretching
832.2	Si-C stretching
746.1	CH_3 in-plane bending
662.4	OH out-of-plane bending

Example spectra of some prepared trimethylsilyl celluloses are shown in *Figure 12*. The signal for Si-C scissoring vibrations at 1248 cm^{-1}, highlighted in grey, is increasing when more trimethylsilyl chloride is used during preparation. Other significant changes represented by bands for O-H stretching, Si-C stretching and conformational ring vibrations can also be observed as mentioned above.

For an estimation of the degree of substitution of the prepared TMSCs, the maximum intensities of the band at 1248 cm^{-1} of commercial TMSC and cellulose were calculated and plotted against the degrees of substitution of these. The obtained function was used as calibration curve based on which the degree of substitution was finally computed. The results of the calculations are shown in *Table 2* and *Figure 13*. As can be seen, the DS_{Si} constantly increases with increasing amount of TMSCl used in preparation with a slight tendency to flatten at higher ratios of silylating agent.

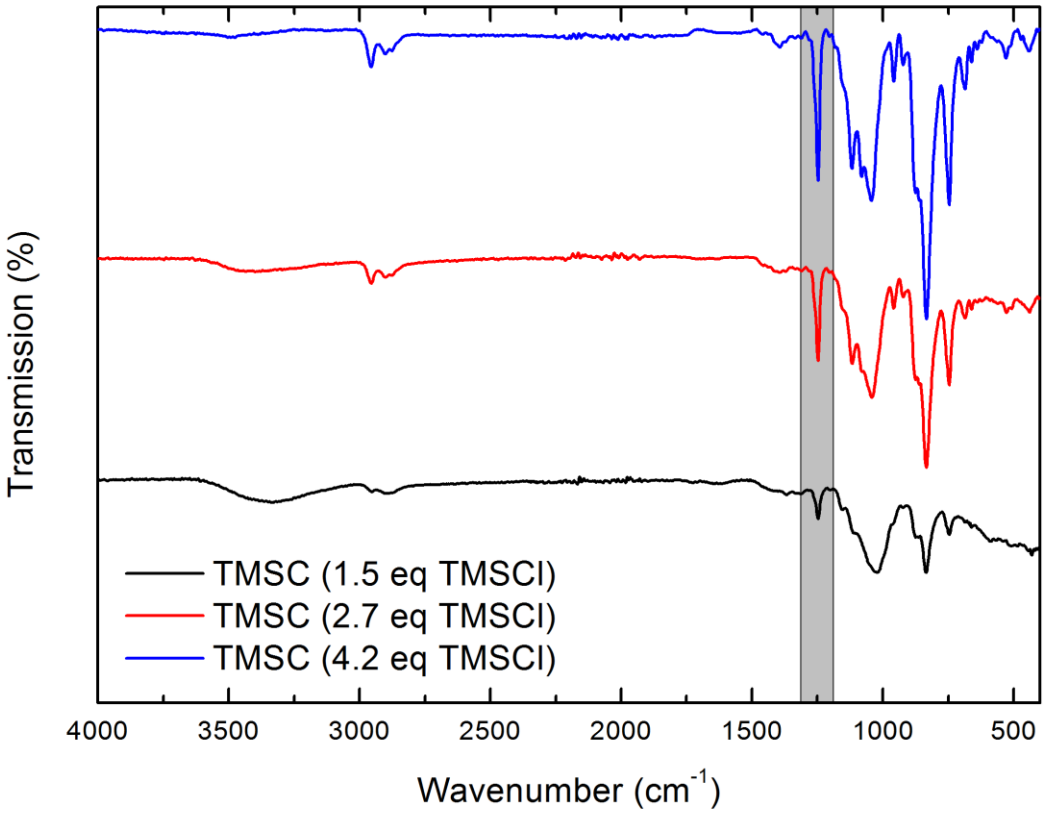

Figure 12. Example spectra of prepared trimethylsilyl celluloses; values in brackets represent the molar ratio of silylating agent compared to AGU achieved by weighing TMSCl prior to silylation

Table 2. Results of solubility tests in comparison to applied ratios of silylating agent and DS_{Si} calculated from IR spectra

Molar ratio		Product		Solubility		
AGU	TMSCl	No.	Calculated DS_{Si}	Ethanol	Ethyl acetate	Chloroform
1	1.0	**1**	0.1	--	--	-- (S)
1	1.5	**2**	0.4	--	--	-- (S)
1	1.7	**3**	0.6	-- (S)	--	-- (S)
1	2.0	**4**	0.9	-- (S)	--	-- (S)
1	2.7	**5**	1.6	--	-- (S)	-- (S)
1	3.1	**6**	1.7	--	--	-- (S)
1	4.0	**7**	2.3	--	--	+
1	4.2	**8**	2.3	--	--	+
1	4.5	**9**	2.6	--	--	+

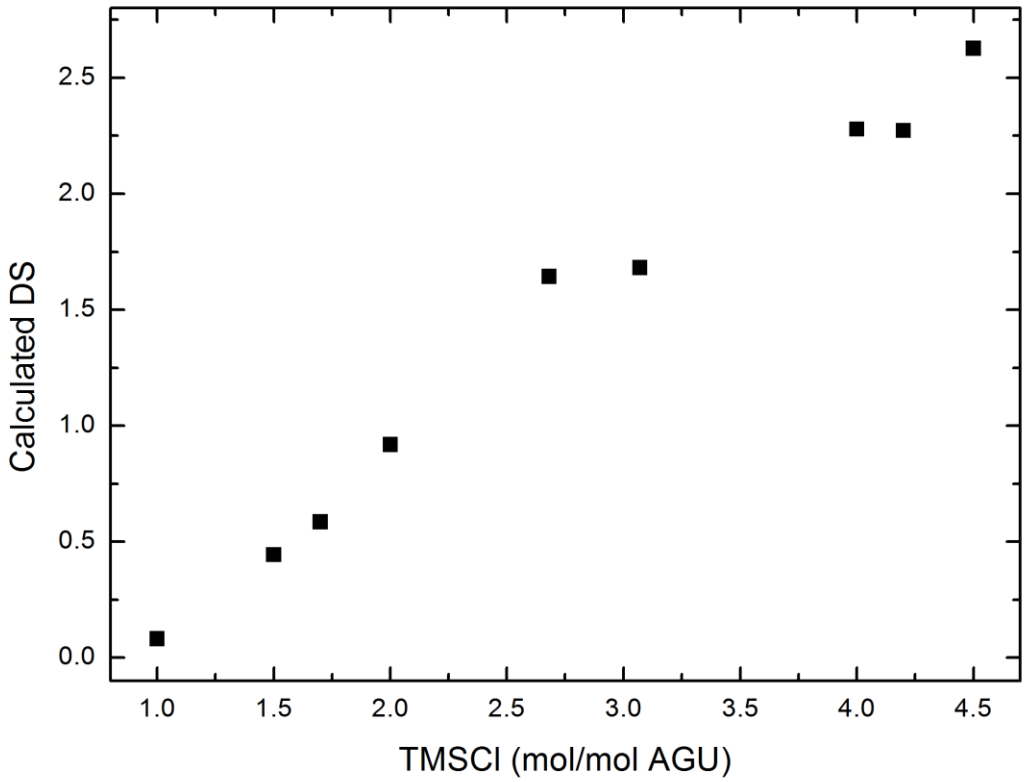

Figure 13. Relation of experimental DS_{Si} values of prepared TMSCs calculated from peak intensities versus the molar ratio of TMSCl to AGU**; * see IR spectra_ Si-CH_3 in-plane bending vibration band at 1248 cm^{-1}, ** achieved by weighing TMSCl prior to silylation*

In the next step the solubility of the products was tested. Based on previous reports in literature, ethanol and ethyl acetate were chosen as "eco-friendly" solvents.[69, 70] As shown in *Table 2*, swelling occurred for trimethylsilyl celluloses featuring several different degrees of substitution, whereas it was not possible to fully dissolve one of the samples. A possible reason for this behaviour could be agglomeration of the polymer chains, due to a high amount of unsubstituted hydroxyl groups. In case of samples **3** and **4,** IR spectra (see *Figure 14*) show small amounts of incorporated water, which could result in a stronger hydrogen bond network and hinder the dissolution of TMSC in ethanol or ethyl acetate. It is feasible as well, that the TMSC regained some degree of crystallinity during the drying process or incomplete dissolution of cellulose prior to preparation led up to remaining crystalline domains within the TMSC. It needs to be pointed out, that the samples with a degree of substitution higher than 2.2 were soluble in chloroform - the solvent used for regeneration experiments - and TMSC with a DS_{Si} below 1.8 showed swelling behaviour.

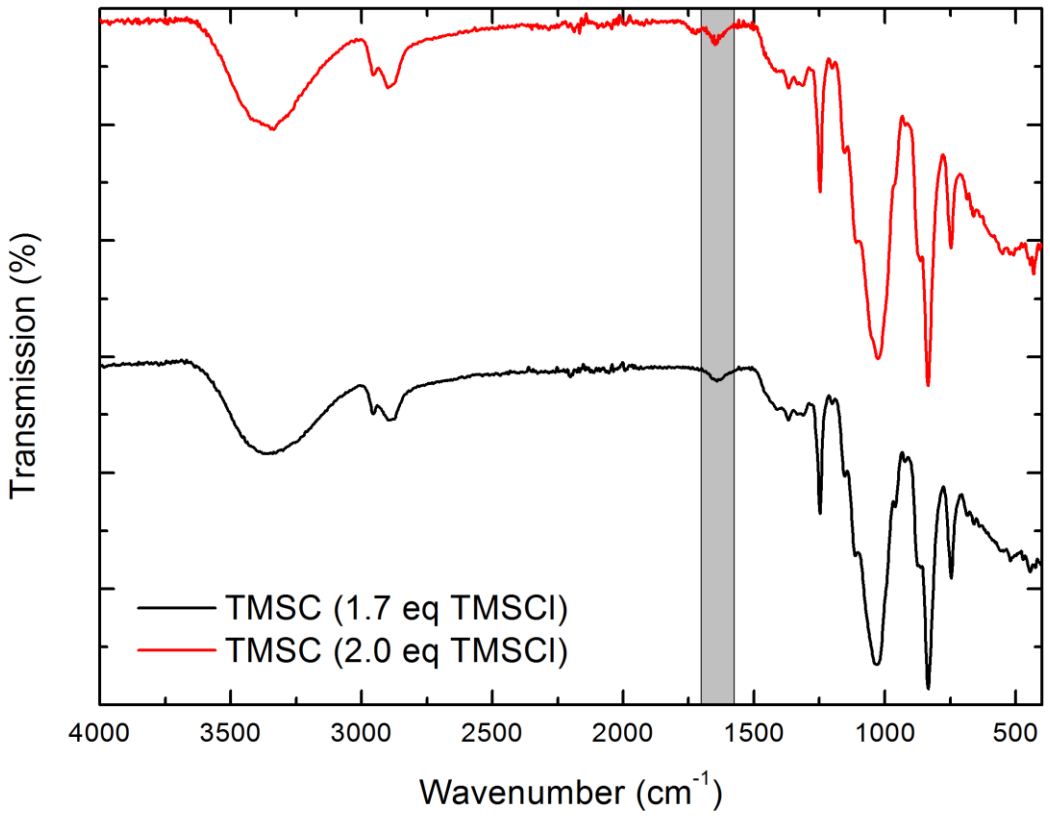

*Figure 14. Comparison of IR spectra of preparated TMSCs **3** and **4** (see Table 2); values in brackets represent the molar ratio of silylating agent compared to AGU achieved by weighing TMSCl prior to silylation; marked area shows location of bands denoting presence of H_2O*

Photoregeneration of cellulose

The other important factor in the regeneration of cellulose, besides the choice of the substrate, is the photoacid generator used and its specific efficiency. Therefore it is necessary to approach the problem from different perspectives - namely the ability to effectively convert TMSC to cellulose and the lamp specific factor of converting light into acid, measured by infrared and UV-visible spectroscopy, respectively. Another point, that cannot be considered negligible, is the morphology of the thin film with respect to further uses, which is investigated by AFM microscopy.

UV-Vis spectroscopy

In the first place, UV-Vis spectra of the tested photoacid generators were recorded (see *Figure 15*) and compared to data prior reported, which is shown in *Table 3*.[43-55] In respect to the measured data, the extinction coefficients were calculated. Approximate locations of absorption maxima were confirmed by the documented values, except for (*Boc*-methoxyphenyl)diphenyl-sulphonium triflate, for which the manufacturers data was used for comparison.

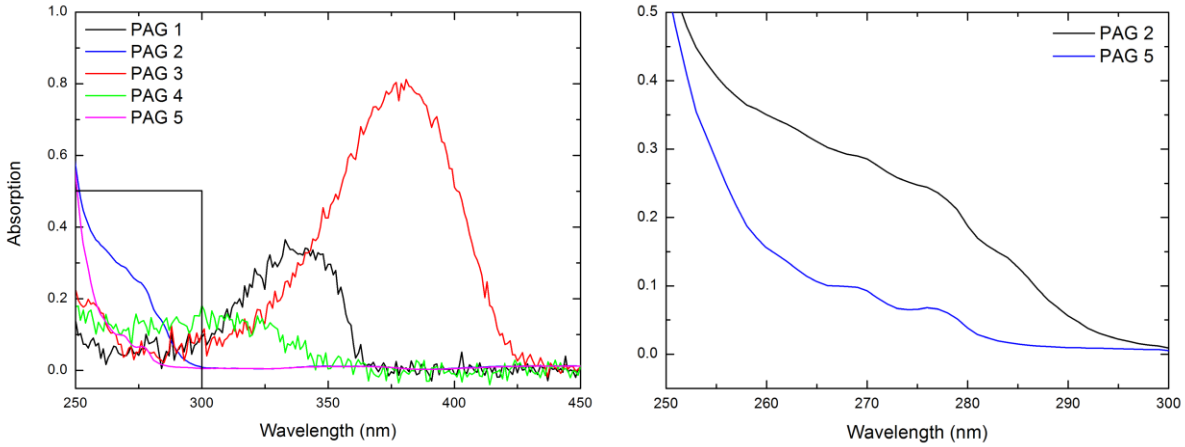

Figure 15. Left: UV-Vis spectra of tested photoacid generators recorded in chloroform at a concentration of 10 µg/ml; right: magnification of the squared area in the picture on the left

Large variances can be observed within the spectral data of the different PAGs both in the wavelengths of maximum absorption and in the amount of absorbed light. Whilst PAG **3** shows a very high absorption of 0.8 at a concentration of 10 µg/ml, the other photoacid generators' abilities to attenuate light are significantly lower. As can be seen in *Figure 15*, it is not possible to evaluate correct locations and values of λ_{max} for PAGs **2** and **5** as well as the valid molar mass of PAG **4**. The underlying reason is, that, in terms of PAGs **2** and **5**, the method of determination does not allow for measurements in the relevant wavelength area because of a high noise level below 250 nm, while PAG **4** consists of a mixture of two different cations, whereby the exact ratio could not be obtained, neither from literature nor from the supplier (see *Figure 4*). This led to a problem in the calculation of the corresponding extinction coefficient and should be the reason for the deviation of the reported and the achieved values as well.

Table 3. Calculated values for the extinction coefficients of different PAGs at wavelengths obtained by described measurement and their comparison to reported values

PAG	λ_{max} / nm	abs	ε / $M^{-1}*L^{-1}$	ε^{a} (λ_{max}^{a}) / $M^{-1}*L^{-1}$
1	341	0.33	11393	10150 (335 nm)
2	--[b]	--[b]	--	-- (255 nm)[c]
3	381	0.80	35837	34000 (370 nm)
4	310	0.14	5201	23400 (225 nm) 19500 (305 nm)
5	--[b]	--[b]	--	18600 (235 nm)

[a] Previously reported data[43-55]

[b] No data achievable

[c] No data reported (λ_{max} taken from supplier)

Table 4. Calculated values for the specific irradiance of different PAGs derived from given formulas (see Experimental section)

PAG	E_e^{spec} / $mW*m^{-2}$
1	1.56
3	6.29
4	1.00

As a possibility to compare photoacid generators, the absorption spectra of PAG **1**, **3** and **4** were used to weight the emission spectrum of the lamp utilized for illumination of the thin films. The values calculated through integration of the obtained functions are noted in *Table 3*. The irradiance data shown is not comparable without considering the different spectral intensities of the lamp's emission and varying absorption areas of the photoacid generators. Regarding that, the ratio between the irradiance calculated and the lamps overall irradiance was used for comparison and is also shown in *Table 4*. As can be seen, PAG **1** and **4** are able to work with very low amounts of energy while PAG **3** is accessing the threefold quantity. Since these values are lamp specific, they are not comparable to literature and the experiments even have to be repeated if the light source is changed.

For further evaluation of this data the conversion rate of TMSC to cellulose has to be taken into account, which is subjected in the next section.

Infrared spectroscopy

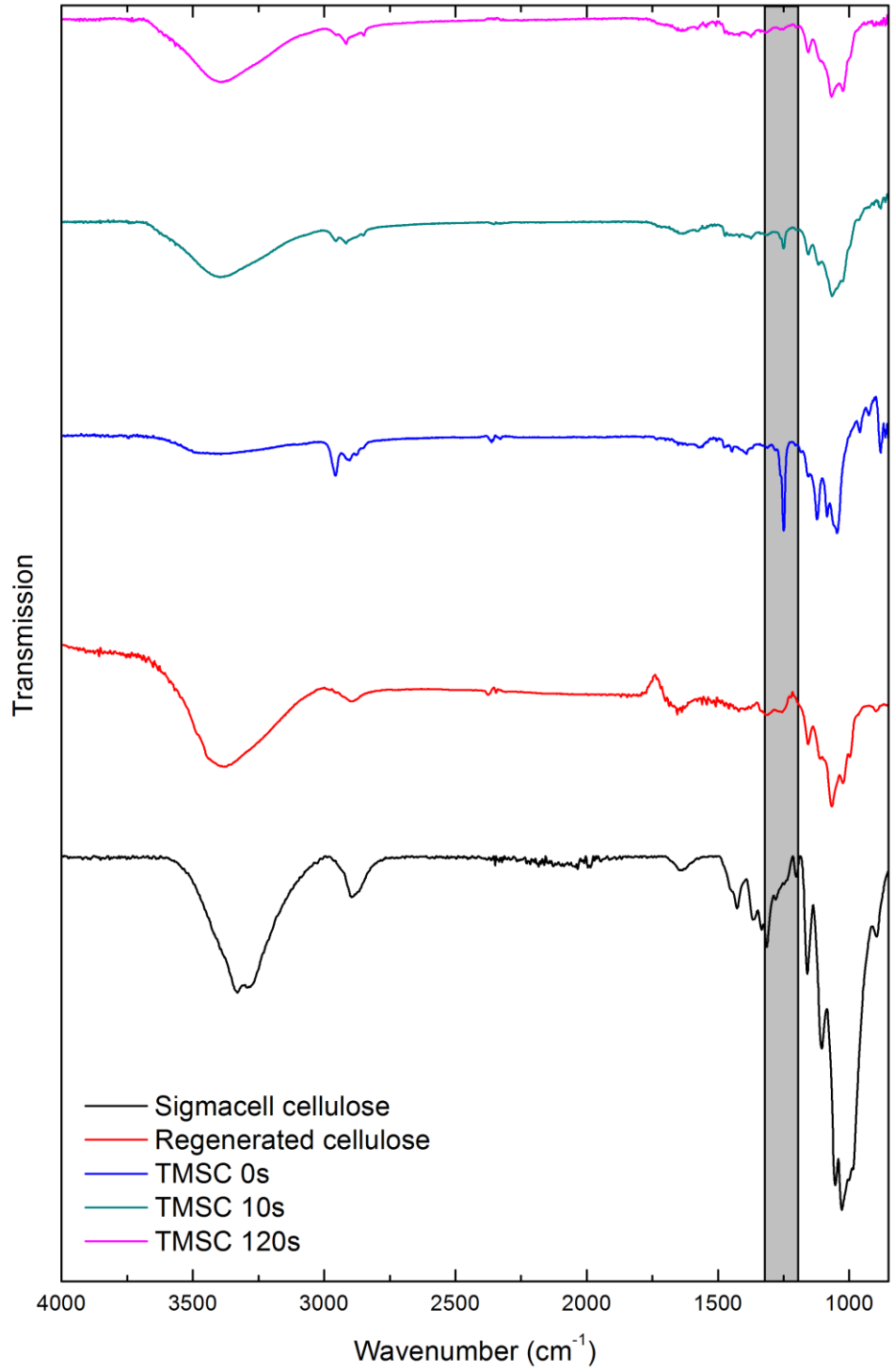

*Figure 16. IR spectra of TMSC containing 15 %(w/w) PAG **4**, Sigmacell cellulose* and cellulose regenerated from commercial TMSC by HCl vapour; time in textbox represents total irradiation time at the time of measurement; marked area highlights location of bands corresponding to silylgroups; * measured with ATR FTIR*

In order to survey the photoacid generators abilities to regenerate cellulose - and therefore generate acid - the process of trimethylsilyl group elimination is followed by infrared spectroscopy. The peak assignment was already stated above and will not be repeated in detail for that reason.

The spectra shown in *Figure 16* represent samples to illustrate the cleavage of TMS groups as well as a comparison between the effects of different routes of regeneration - namely hydrochloric acid vapours and photoacid generators. As can be seen, the peak for Si-C bending vibrations at 1248 cm^{-1} significantly decreases over the course of continuous illumination. Since infrared transmission of CaF_2 substrates is virtually zero at wavenumbers below 850 cm^{-1}, the second signal belonging to Si-C stretching vibrations cannot be taken into account.

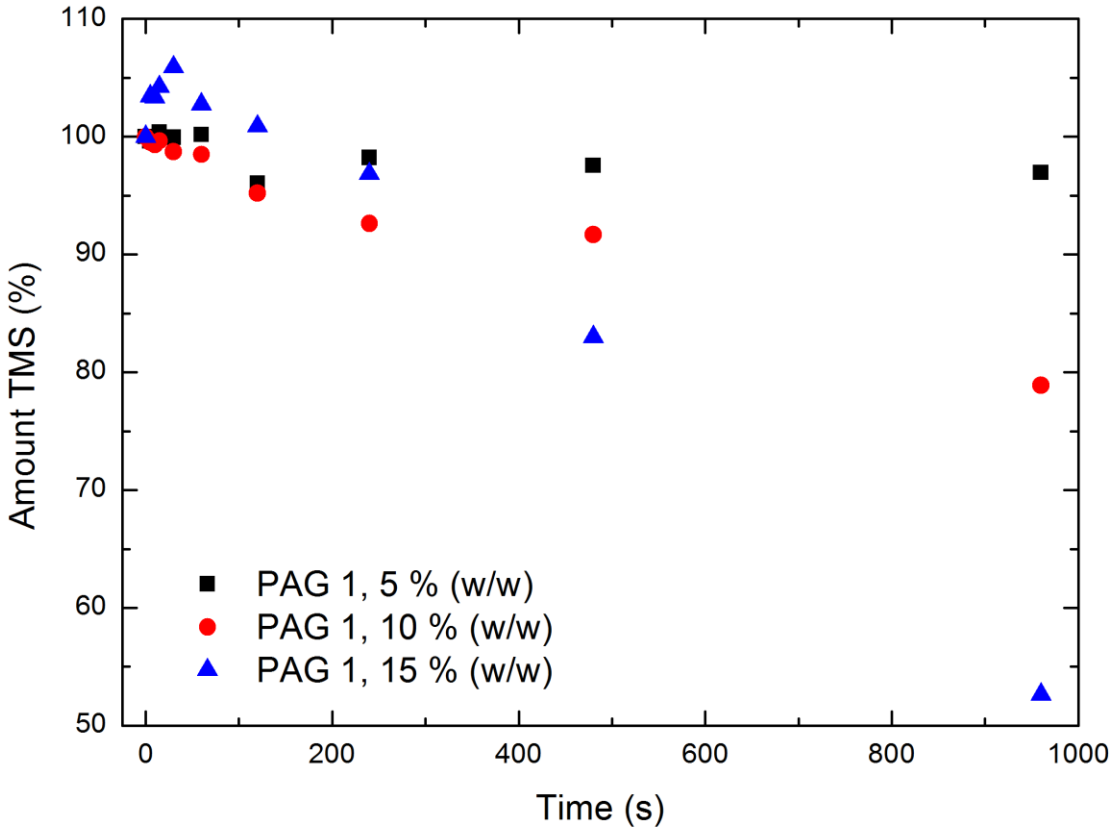

*Figure 17. Process of cleavage of TMS groups from TMSC thin films containing 5 %(w/w), 10 %(w/w) and 15 %(w/w) PAG **1**, respectively; the amount of remaining TMS groups has been determined by IR spectroscopy*

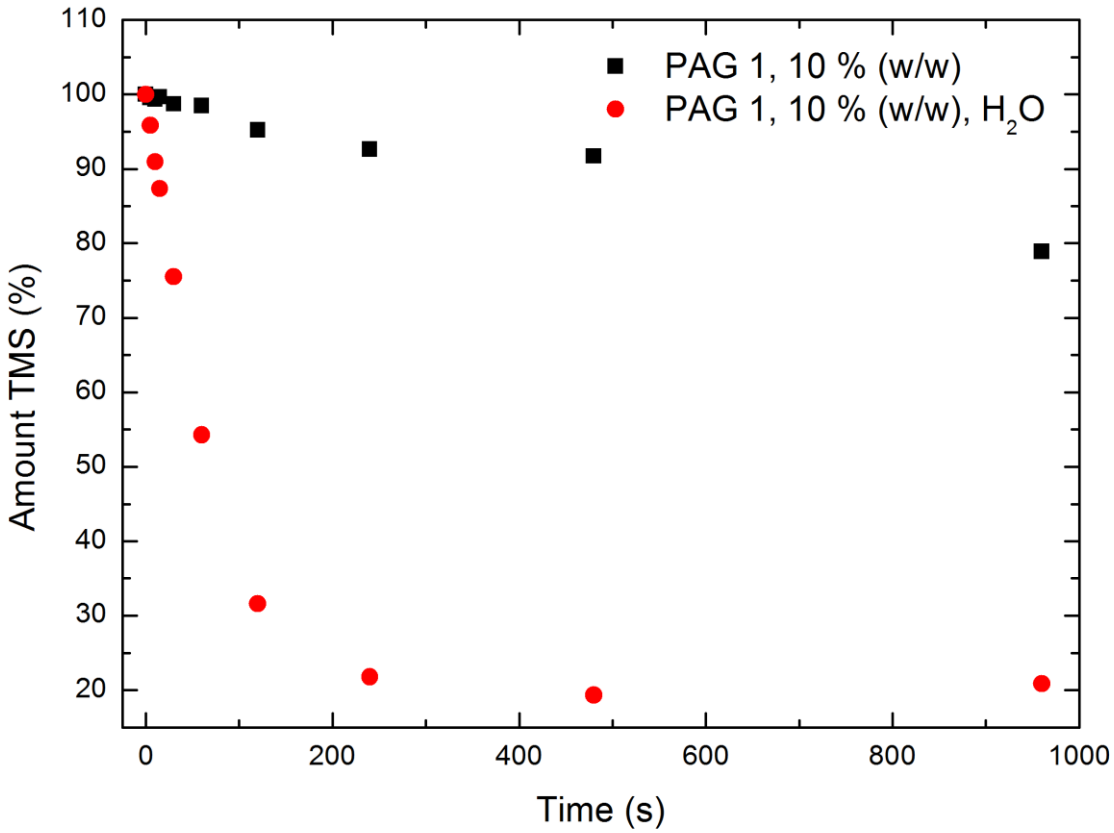

*Figure 18. Kinetics comparison of samples containing PAG **1** at a concentration of 10 %(w/w), effect of humidity during photoregeneration of the films; H_2O denotes the sample, where humidity saturated atmosphere was created*

Compared to conventionally regenerated cellulose, the cellulose obtained via photoacid generators exhibits similar peak intensities for silicon bands and therefore it is assumed that both techniques are capable of fully converting TMSC to cellulose. This can also be confirmed by comparing said spectra with the spectrum of commercial, microcrystalline cellulose even though the signals for ring conformation vibrations vary widely.

A possible explanation for the variations mentioned before could be morphological differences between the measured samples. More precisely, trimethylsilyl cellulose was spin coated onto the substrates and as a result the molecules are in an amorphous state, while the commercial cellulose has ordered, crystalline areas, which may show different absorption behaviour due to strong intermolecular interactions. It has already been stated, that regeneration of cellulose leads to reformation of hydrogen bonds resulting in cellulose II crystal structure, whereas commercial, microcrystalline cellulose obtained from natural sources (e.g. plant, bacteria) mainly consists of

cellulose I. The most obvious variations in IR spectra can be found in the area of OH-stretching vibrations, where the native cellulose I allows for an approximate distinction of different hydroxyl groups, which cannot be observed in the case of regenerated cellulose, due to strong overlapping (see *Figure 16*).[71]

Leading from this argumentation, in the next step the different photoacid generators are compared to each other. For this reason the consecutive spectra measured over a definite period of time are used to calculate the peak heights of the Si-C signal at 1248 cm^{-1}. The values obtained this way indicate the amount of silicon protecting groups remaining in the investigated thin film and consequently the completeness of regeneration to cellulose.

The aforementioned time-dependent course of regeneration can now be displayed by plotting these values against the specific illumination time. Starting with PAG **1**, *N*-hydroxynaphthalimide triflate, the graphs shown in *Figure 17* could be achieved. Typically, an exponential decay can be

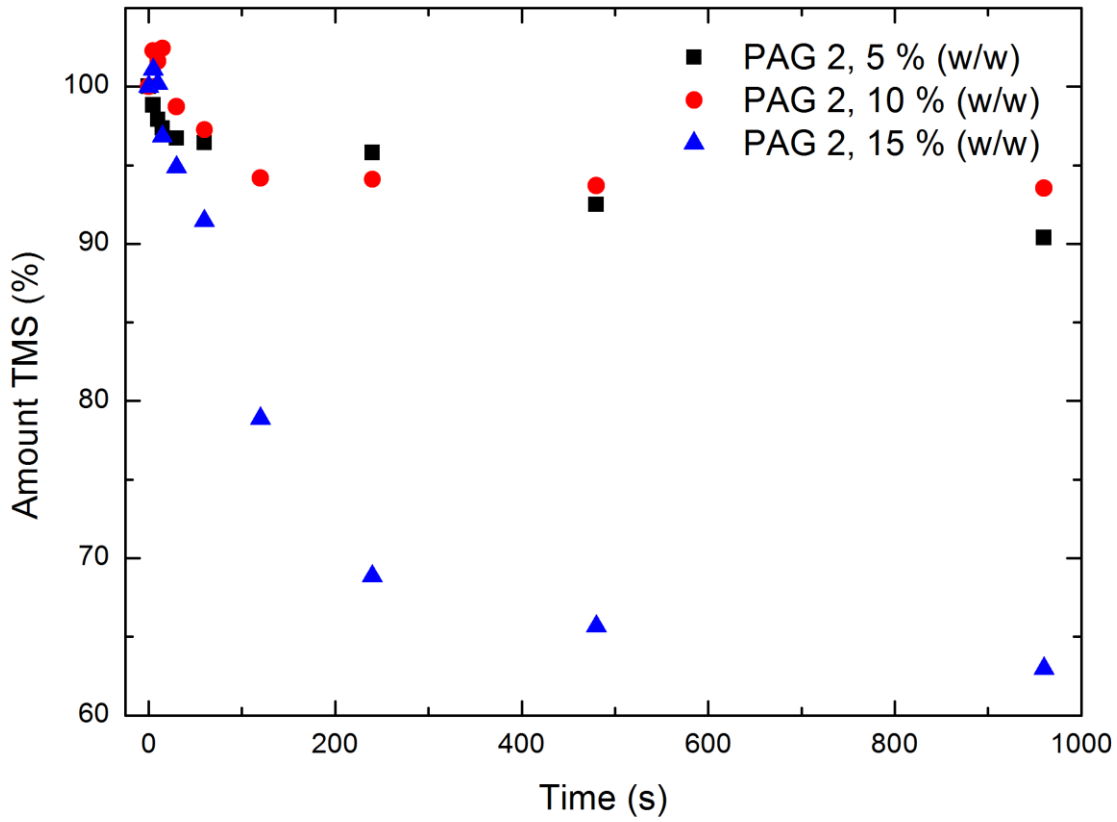

*Figure 19. Process of cleavage of TMS groups from TMSC thin films containing 5 %(w/w), 10 %(w/w) and 15 %(w/w) PAG **2**, respectively; the amount of remaining TMS groups has been determined by IR spectroscopy*

expected, but was not observed in this particular case. Since this photoacid generator is known to work properly from previous research[72], all experiments were repeated without major improvement being acquired. After several tests, the reason for this behaviour was figured out: a lack of hydrogen sources for acid generation. By adding water into the spin coater, the humidity in the coating chamber was artificially increased, leading to higher content of water in the film. Based on this procedure the data shown in *Figure 18* could be obtained. As can be seen, the amount of remaining silicon in the film decreases to approximately 20 % within 4 minutes, whereas the former sample stayed above 90 % in the same period of time.

In contrast to PAG **1**, PAG **2** shows the expected exponential decay, but the overall performance is much lower as *Figure 19* indicates; these observations will be discussed with PAG **4** and **5**. Similar acid generation capabilities were also found for PAG **3**. This fact can be explained by the low quantum yield of this specific due to an extended chromophore, which has already been reported by Pohlers et al.[46-48] Corresponding graphs are shown in *Figure 20*.

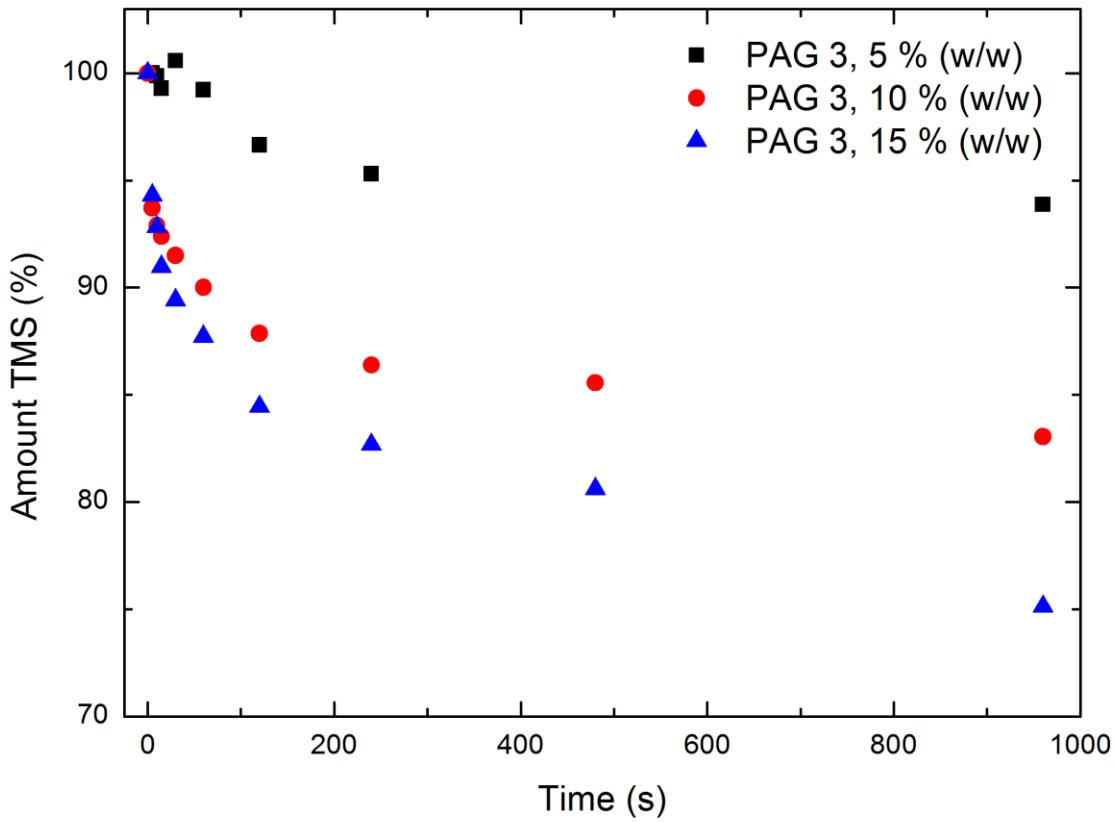

*Figure 20. Process of cleavage of TMS groups from TMSC thin films containing 5 %(w/w), 10 %(w/w) and 15 %(w/w) PAG **3**, respectively; the amount of remaining TMS groups has been determined by IR spectroscopy*

PAG **4** offers the best performance of the photoacid generators within the scope of this work. As can be seen in *Figure 21* the amount of remaining organosilicon protecting groups reaches 20 % at a concentration of 10 %(w/w). Unlike PAG **1**, this extent of efficiency could be achieved without supporting appliances, which favours the application of this salt. Assuming same improvability through simple methods as for *N*-hydroxynaphthalimide triflate, this photoacid generator has a high potential for further improvement towards lower concentrations.

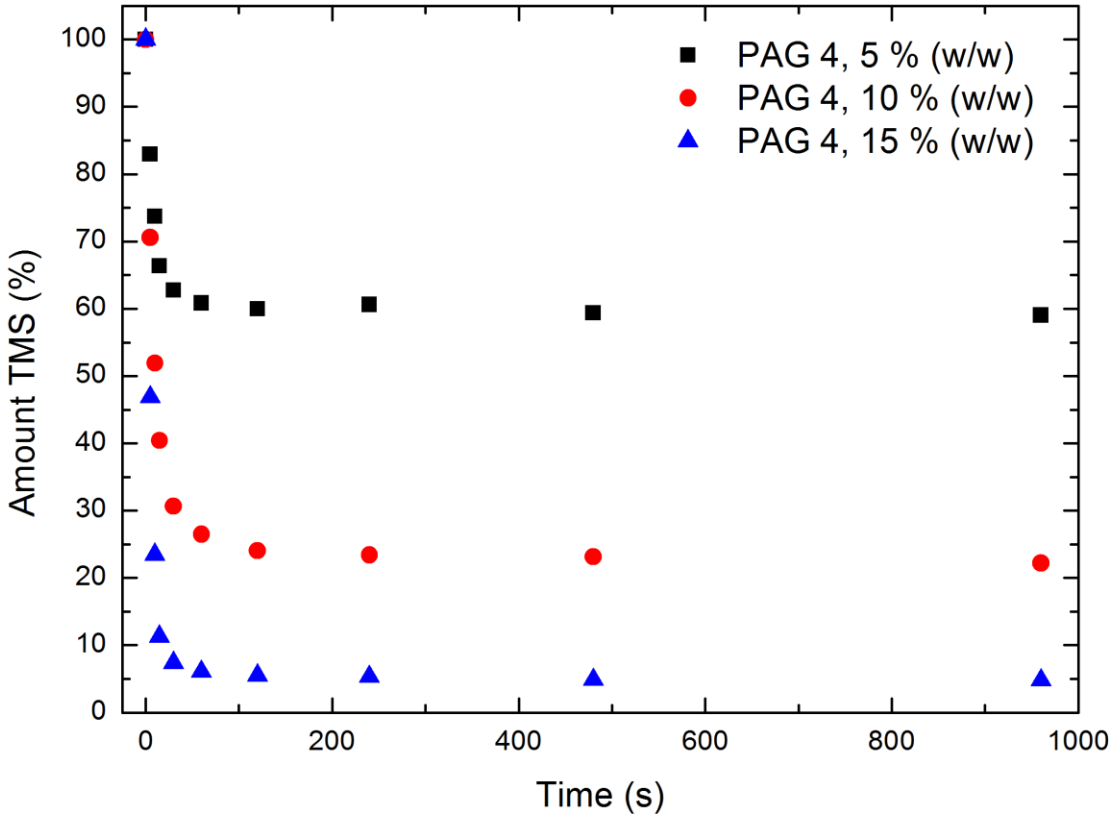

*Figure 21. Process of cleavage of TMS groups from TMSC thin films containing 5 %(w/w), 10 %(w/w) and 15 %(w/w) PAG **4**, respectively; the amount of remaining TMS groups has been determined by IR spectroscopy*

The last PAG to review in this series of tests is triphenylsulphonium triflate, the parent compound to PAG **2** and **4**. It is clearly evident from *Figure 22* that PAG **5** is less efficient than PAG **4**, but more efficient than PAG **2**. Previous research concerning the influence of substitution on the aryl groups claimed, that electron donating substituents (e.g. alkoxy-groups) are able to lower the efficiency by 30-40, except for phenylthio moieties, which can increase the amount of acid generated to 112 % compared to the unsubstituted sulphonium salt. Scientists assume the reason

for this behaviour to be a combination of singlet state stabilisation and an increased rate of inter system crossing. [49-55]

As can be seen from the previous section, the same experiments as described here were also conducted with samples containing a lower amount of photoacid generator.

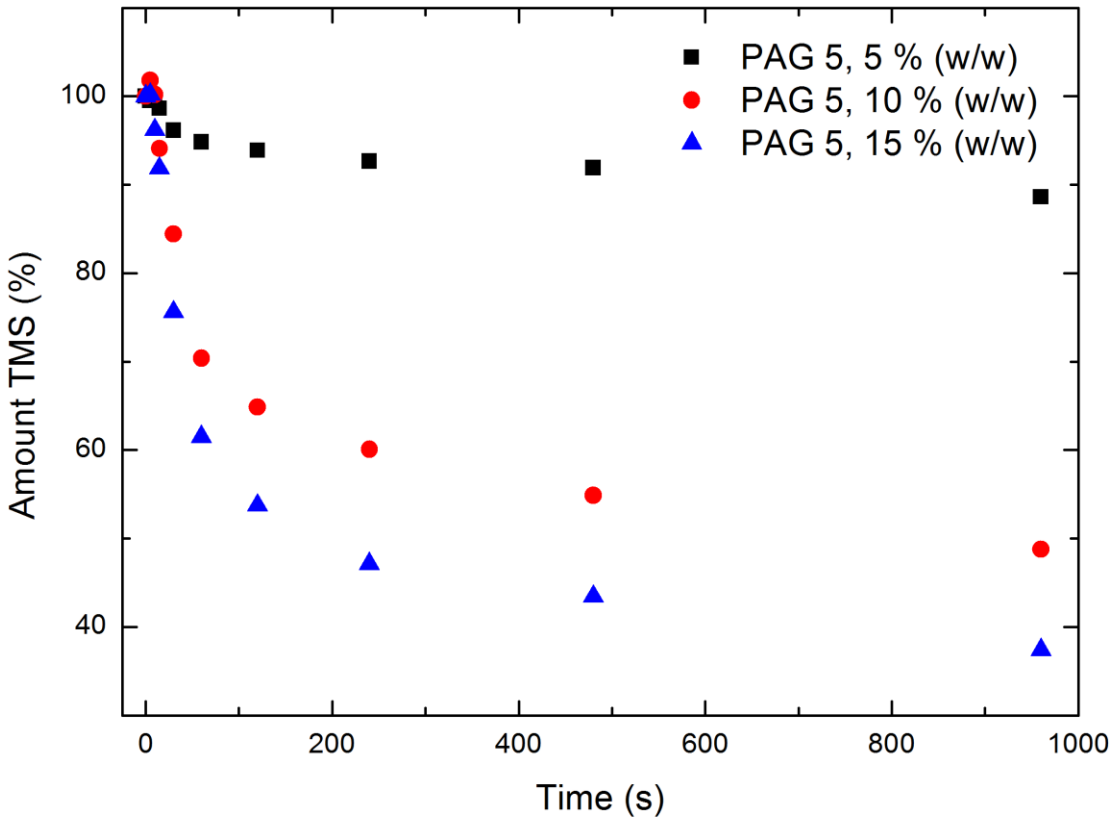

*Figure 22. Process of cleavage of TMS groups from TMSC thin films containing 5 %(w/w), 10 %(w/w) and 15 %(w/w) PAG **5**, respectively; the amount of remaining TMS groups has been determined by IR spectroscopy*

Since one of the targets of this work is the achievement of a sustainable method for the structuring of cellulose thin films, the same experiments as described here, were also conducted with samples containing a lower amount of photoacid generator, as denoted in the previous section. As an example, *Figure 23* shall show the subsequent loss of trimethylsilyl groups over the course of the experiment of PAG **4** at concentrations of 1 %(w/w) and 2 %(w/w) relative to the amount of TMSC in the spinning solution. Compared to higher concentrations, it can be seen, that the performance is drastically decreased, yielding a 10-fold difference between samples

containing 2 %(w/w) and 5 %(w/w) photoacid generator. In case of the other PAGs, the results seem to be even worse, what can be seen in *Figure 24* to *Figure 27* on the following pages. However, one observation, that has to be mentioned, is an increase in the amount of remaining trimethylsilyl groups, which can be found in the data of each sample at low PAG concentrations. The most probable explanation is the attainment of the detection limit, since IR spectroscopy is applied to track the experiments. The infrared bands used to detect silicon are located at 1248 cm^{-1} in the fingerprint region and therefore can easily be superposed by other vibrational signals, leading to small interferences in the spectrum. Furthermore, the CaF_2 substrates account for additional signal noise. These reasons do not allow for plausible interpretation of data concerning very small alterations of the total silicon content.

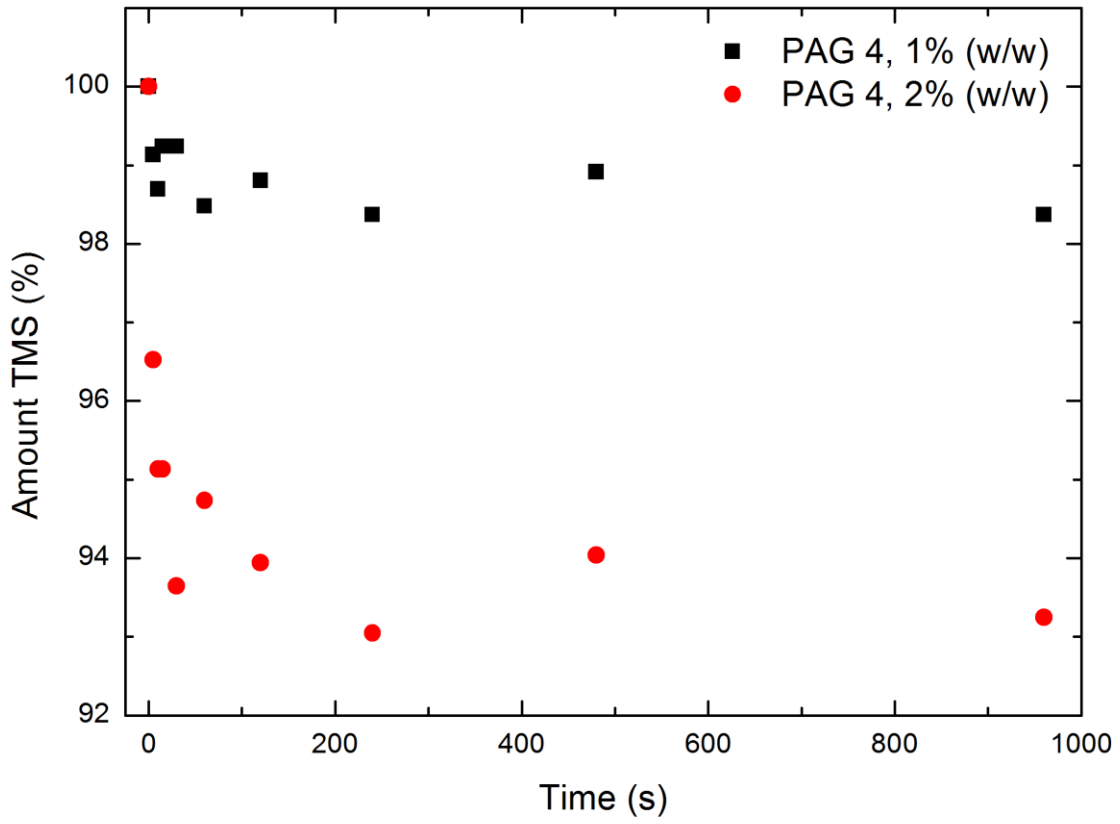

*Figure 23. Process of cleavage of TMS groups from TMSC thin films containing 1 %(w/w) and 2 %(w/w) PAG **4**, respectively; the amount of remaining TMS groups has been determined by IR spectroscopy*

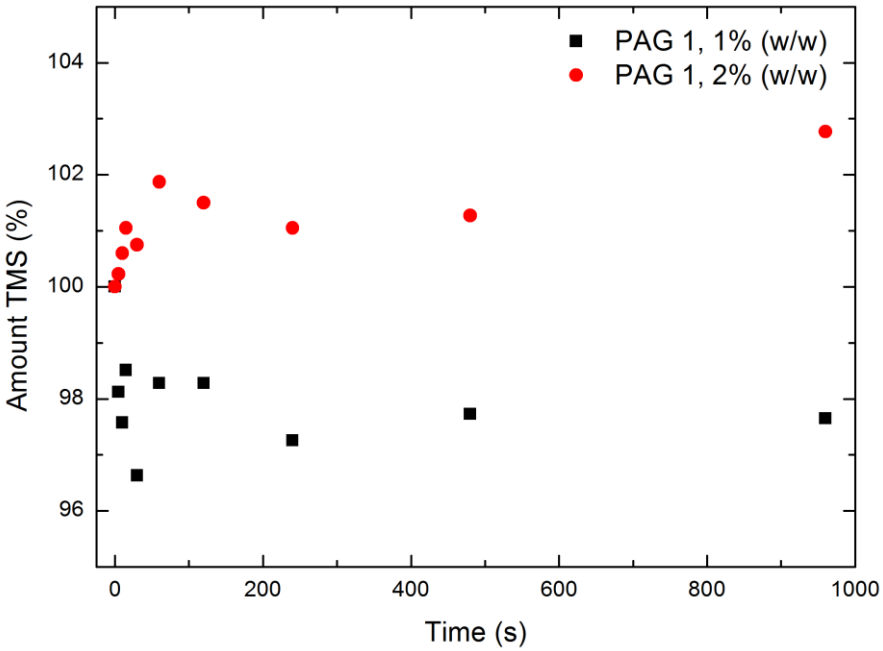

*Figure 24. Process of cleavage of TMS groups from TMSC thin films containing 1 %(w/w) and 2 %(w/w) PAG **1**, respectively; the amount of remaining TMS groups has been determined by IR spectroscopy*

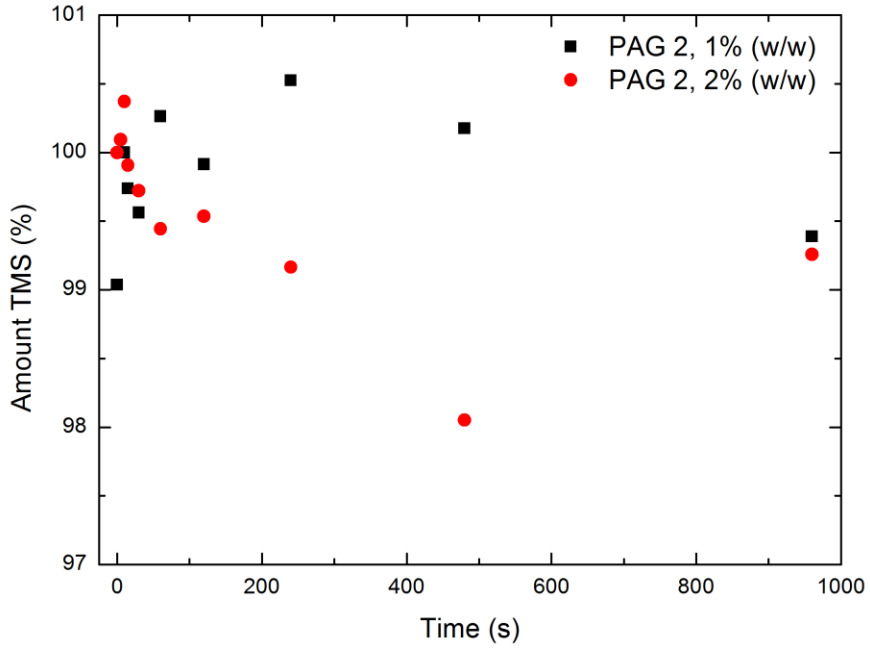

*Figure 25. Process of cleavage of TMS groups from TMSC thin films containing 1 %(w/w) and 2 %(w/w) PAG **2**, respectively; the amount of remaining TMS groups has been determined by IR spectroscopy*

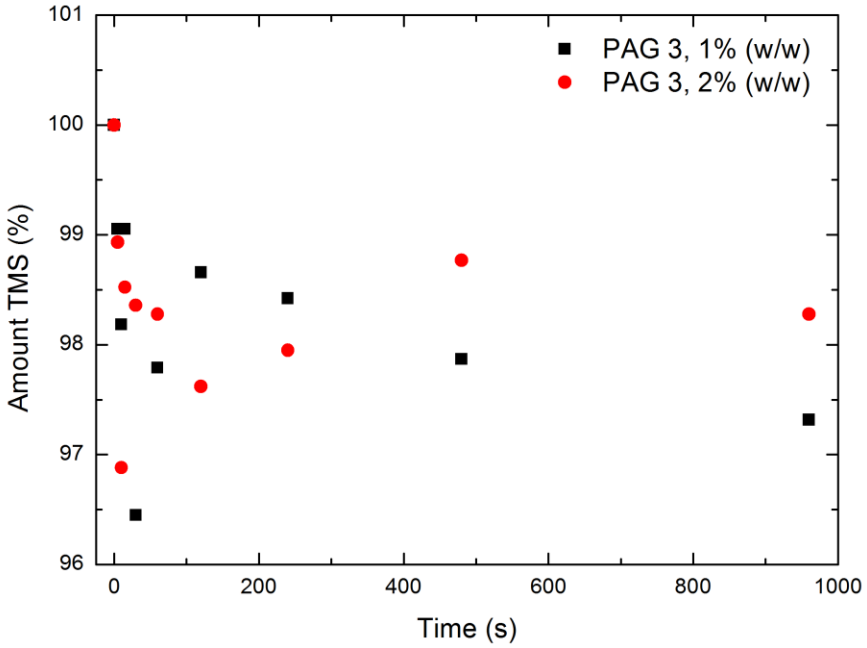

*Figure 26. Process of cleavage of TMS groups from TMSC thin films containing 1 %(w/w) and 2 %(w/w) PAG **3**, respectively; the amount of remaining TMS groups has been determined by IR spectroscopy*

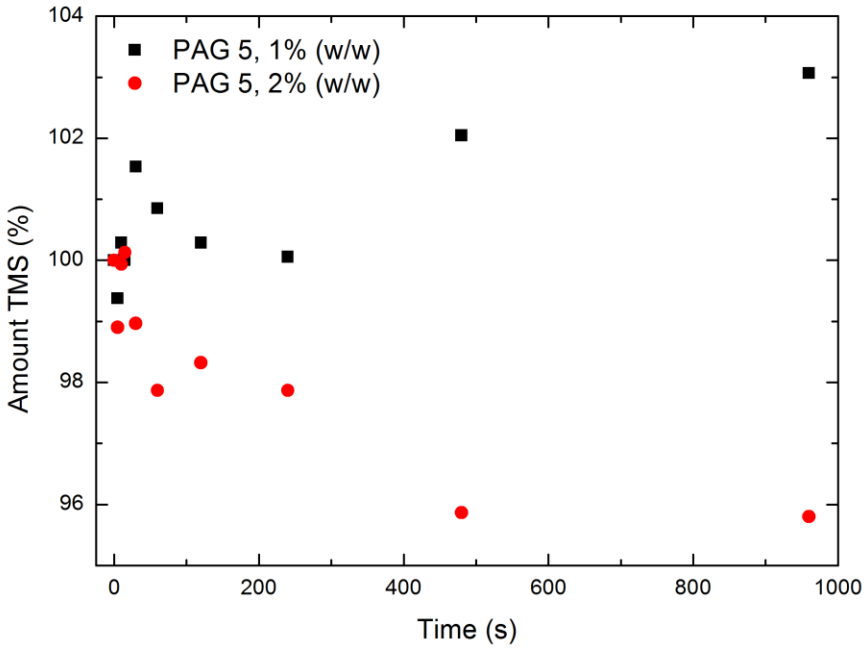

*Figure 27. Process of cleavage of TMS groups from TMSC thin films containing 1 %(w/w) and 2 %(w/w) PAG **5**, respectively; the amount of remaining TMS groups has been determined by IR spectroscopy*

Atomic force microscopy

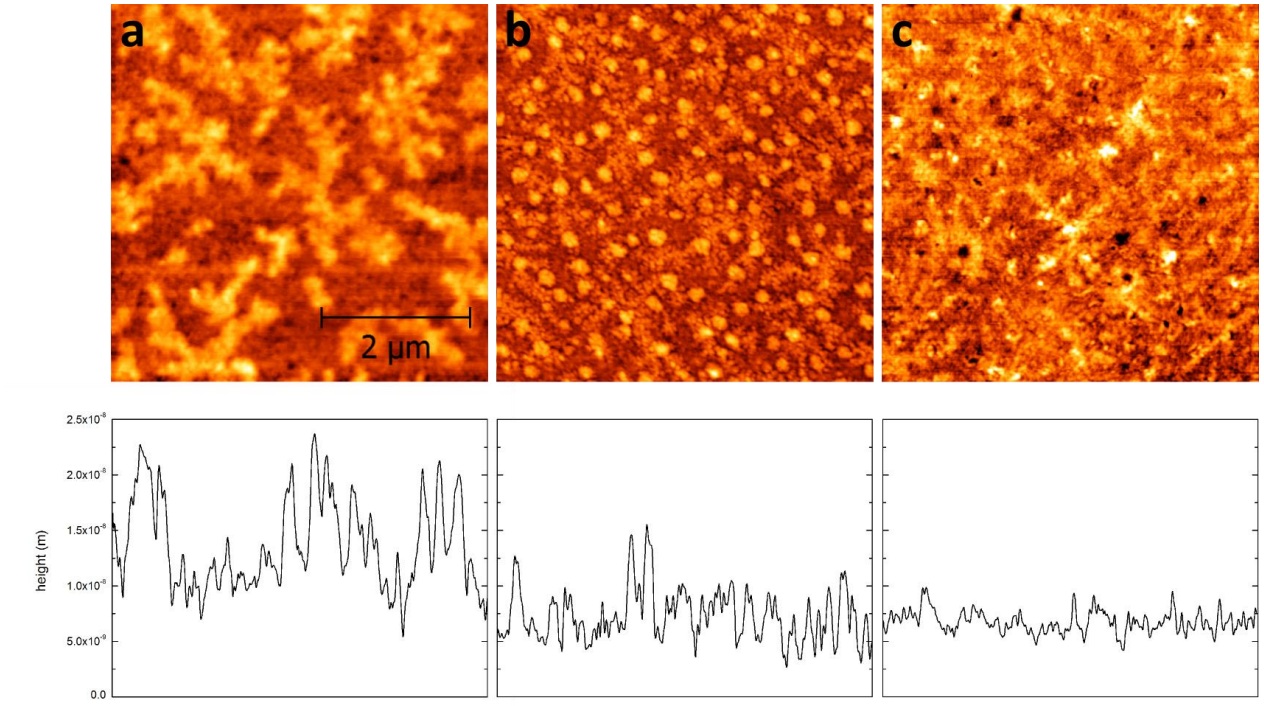

*Figure 28. AFM micrographs recorded before illumination (a), after illumination (b) and after developement (c) and corresponding height profiles of PAG **1**; height profiles represent data on the diagonal from upper, left to lower right corner*

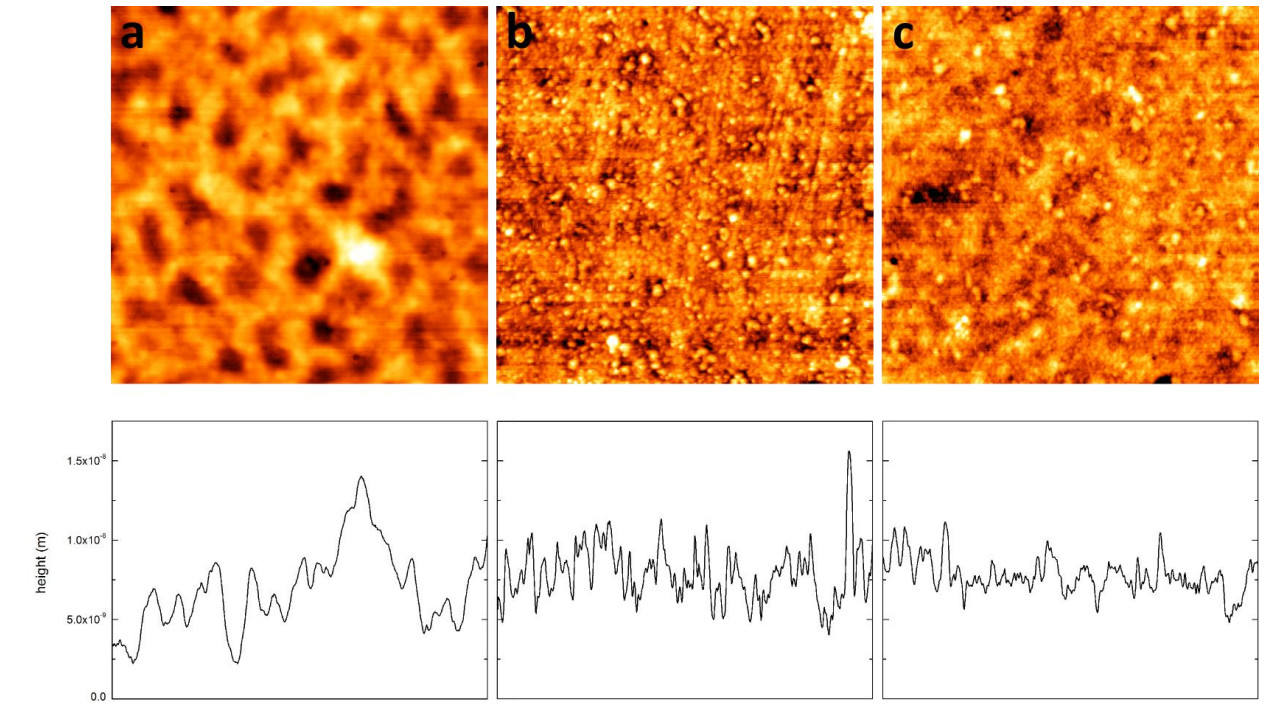

*Figure 29. AFM micrographs recorded before illumination (a), after illumination (b) and after developement (c) and corresponding height profiles of PAG **2**; height profiles represent data on the diagonal from upper, left to lower right corner*

For the utilisation of regenerated cellulose in microelectronics or related areas of application it is important to be aware of several characteristic processes occurring during regeneration. These morphological changes can be traced by measurement of roughness and thickness of the deposited films over the course of the experiment. In the scope of this work mentioned alterations were observed by tapping mode atomic force microscopy.

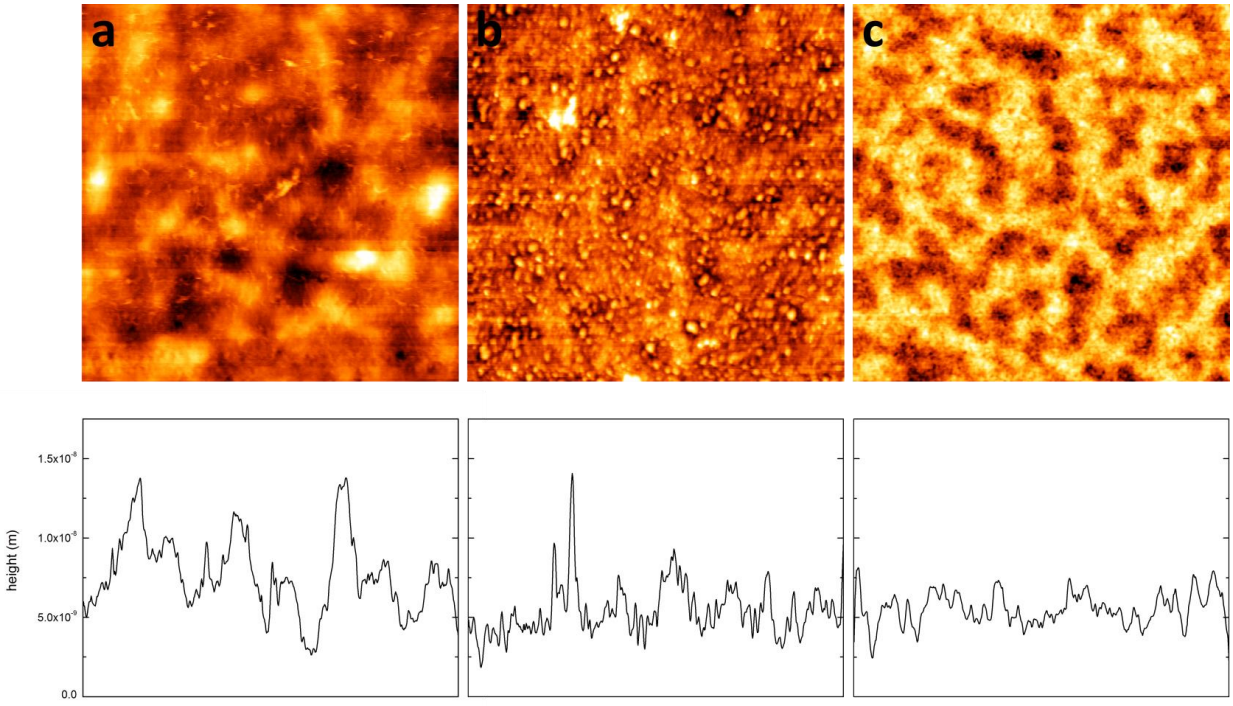

*Figure 30. AFM micrographs recorded before illumination (a), after illumination (b) and after developement (c) and corresponding height profiles of PAG **5**; height profiles represent data on the diagonal from upper, left to lower right corner*

As can be seen in *Figure 28* to *Figure 30*, the surface structure of the tested samples is clearly changing. One aspect that has to be considered regarding the morphology, is directly related to the presence of photoacid generators in the thin films. The amorphous structure of the layer can be further disturbed by photoacid generator molecules disrupting the possibility of rigid TMSC chains lying flat. In the case of PAG **1**, the high crystallinity of the compound itself combined with high concentrations should be the reason for the formation of aggregates on the surface, since this effect is drastically reduced with decreased concentration. This proposal is further supported by data presented in *Figure 31*. The thickness of the sample containing PAG **1** is reduced by 50 %, whereas the roughness is not affected during illumination and does not change before treatment of the photoregenerated layer with chloroform, which causes dissolution of the photoacid

generator. Contrary behaviour in terms of alterations in roughness can be seen, when comparing then thin films containing the other PAGs. Development of the samples leads to surface smoothing, even if the photoregeneration process generates first effects. Except for PAG **1**, the changes in surface conditions occurring during UV-light irradiation can easily be explained by elimination of protecting groups and therefore morphological modifications of the thin film arise. The reconversion of TMSC to cellulose causes a reformation of hydrogen bridge bonds providing a drastical increase in density. In order to facilitate this, the thickness of the layer decreases by 50 to 60 %, which has already been stated.[16, 73-76]

As mentioned before, the surface morphology of the sample containing PAG **1** is mainly caused by the photoacid generator itself in contrast to films incorporating PAG **2** or **5**, which can be seen in *Figure 28* to *Figure 30*. The latter show close resemblance to each other before development, which is illustrated by the structural similarity of these photoacid generators. A possible explanation for differences in *Figure 29* c and *Figure 30* c may be the diverse efficiency since PAG **5** is 5 times as efficient as PAG **2** at given concentrations. Remarkably, thickness of films created with sulphonium salt photoacid generators differ by about 5 %, while variations in roughness amount to 14 %, despite the different appearance of the final product.

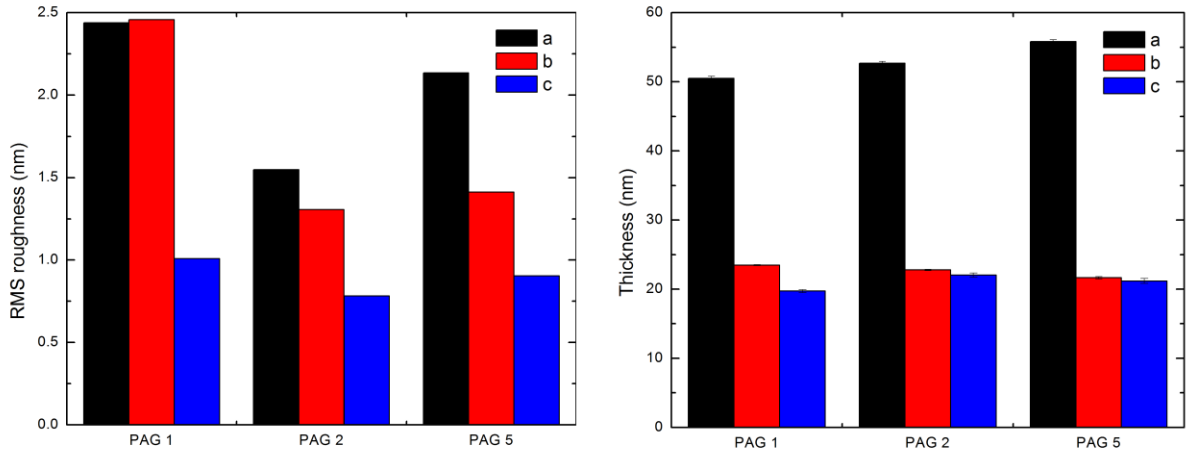

Figure 31. Comparison of RMS roughness and thickness of depicted PAGs over the course of the experiment (before illumination (a), after illumination (b), after development (c))

Contact angle measurement

From the results of static contact angle measurements with water (see *Table 5*), which are depicted in *Figure 26*, it can be seen that the values change by about 5 % in the course of illumination for both photoacid generators. This can be described by PAG decomposition products diffusing to the surface of the cellulose film during regeneration due to the increase of density and therefore the contraction of the film. When the sample is submerged in chloroform, thus developed, the static contact angle is clearly changing, what is the necessary consequence of the dissolution and therefore the removal of hydrophobic remains. In fact, the values do decrease, but not in a sufficient manner, if compared to previously reported data.[18, 20, 75] A possible reason for this observation could be incomplete regeneration; remaining trimethylsilyl groups on the surface are likely to increase the measured static contact angles. However, the results of this method confirm a successful regeneration process.

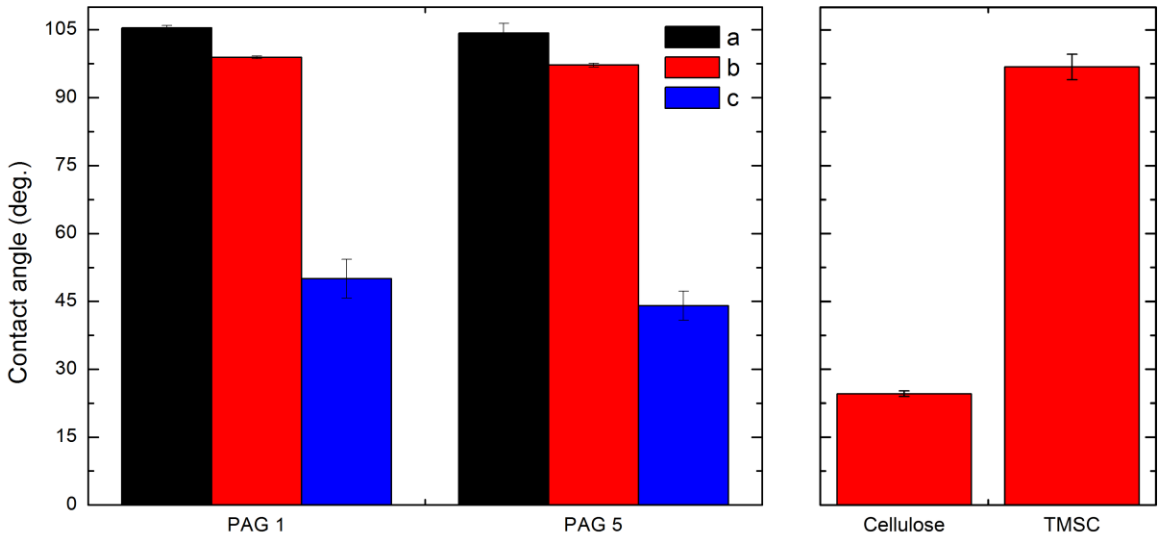

Figure 32. Left: static contact angles of samples containing 10 %(w/w) of depicted PAGs (before illumination (a), after illumination (b), after development (c)), right: static contact angles of TMSC and regenerated cellulose thin films previously reportet[15, 69]; implied data can be found in Table 5

Table 5. Mean static contact angles measured with water, each calculated from 3 individual measurements.

	non-illuminated / deg	illuminated / deg	developed / deg
PAG **1**	105 ± 0.6	99 ± 0.3	50 ± 4.3
PAG **6**	104 ± 2.1	97 ± 0.4	44 ± 3.3

Conclusion & outlook

Concerning the silylation of cellulose it has been shown that a broad variety of TMSCs referring to their degree of substitution can be achieved even with a convenient and straightforward method such as the one used in the course of this work. The lack of solubility of the synthesised cellulose derivatives in “eco-friendly” solvents is a problem that still needs to be addressed. A possible explanation for this behaviour is poor dissolution of cellulose in the DMA/LiCl mixture due to insufficient activation methods or purity issues. The removal of potential residual moisture, which was detected in some of the samples, represents another promising option. Since changes to the procedure regarding the mentioned possibilities are laborious or expensive, other ways of improvement need to be found in order to create a material for new and sustainable applications.

The investigations regarding the efficiency of photoacid generators produced varying results. On the one hand *Boc*-methoxyphenyldiphenylsulphonium triflate (PAG **2**) and 2-(4-Methoxystyryl)-4,6-bis-(trichloro-methyl)-1,3,5-triazine (PAG **3**) performed poorly in the given environment, which could be explained by substituent effects. Since their efficiency and quantum yields are too low compared to other photoacid generators, further application for regeneration tasks is not favoured. While laboratory findings of triphenylsulphonium triflate (PAG **5**) were mediocre, the performance of the two remaining PAGs seems to be superior. The acquired data concerning *N*-hydroxynaphthalimide triflate (PAG **1**) and triarylsulphonium hexafluoroantimonate salts (PAG **4**) makes these compounds being promising starting points for further research. Nonetheless some improvements need to be made in terms of high photoacid generator concentrations and resulting film properties, whereby it has to be considered that these variables affect each other and they are able to alter the final outcome.

Bibliography

1 D. Klemm, H.-P. Schmauder, T. Heinze, *Biopolymers*, Vol. 6 (Eds.: E. Vandamme, S. De Beats, A. Steinbüchel), Wiley-VCH, Weinheim, **2002**, pp. 277-312

2 M. B. Sticklen, *Nature Reviews Genetics* **2008**, 9, 433-443

3 N. Carpita, M. McCann, *Biochemistry & Molecular Biology of Plants* (Eds.: B. Buchanan, W. Gruissem, R. L. Jones), John Wiley & Sons, New Jersey, **2002**, pp. 52-109

4 D. Klemm, B. Heublein, H.-P. Fink, A. Bohn, *Angew. Chem. Int. Ed.* **2005**, 44, 3358-3393

5 A. Payen, *C. R. Hebd. Seances Acad. Sci.* **1838**, 7, 1052; A. Payen, *C. R. Hebd. Seances Acad. Sci.* **1838**, 7, 1125

6 H. Staudinger, *Ber. dtsch. Chem. Ges.* **1920**, 53, 1073-1085

7 C. F. Schönbein, *Bericht über die Verhandlungen der Naturforschenden Gesellschaft in Basel* **1846**, 7, 26-27 and 27

8 E. Schweizer, *J. Prakt. Chem.* **1857**, 72, 109-111

9 P. Schützenberger, *C. R. Hebd. Seances Acad. Sci.* **1865**, 61, 485-486

10 C. F. Cross, B. T. Bevan, C. Beadle, *Ber. Dtsch. Chem. Ges.* **1893**, 26, 1090-1097 and 2520-2533

11 K. Götze, *Chemiefasern nach dem Viskoseverfahren*, 3rd Edition, Springer, Berlin, **1967**

12 R. Carlisle, *Scientific American Inventions and Discoveries*, John Wiley & Sons, New Jersey, **2004**, p. 338

13 A. Parén, P. Vapaaoksa, *US. Patent* 5417752, **1995**

14 G. Greber, O. Paschinger, *DE Patent* 3104531 **1981**

15 G. Greber, O. Paschinger, *Lenz. Ber.* **1983**, 55, 20-25

16 A. Wolfberger, R. Kargl, T. Griesser, S. Spirk, *Molecules* **2014**, 19, 16266-16273

17 G. K. Cooper, K. R. Sandberg, J. F. Hinck, *J. Appl. Polym. Sci.* **1981**, 26, 3827-3836

18 M. Schaub, G. Wenz, G. Wegner, A. Stein, D. Klemm, *Adv. Mater.* **1993**, 5, 919-922

19 H. A. Schuyten, J. W. Weaver, J. David Reid, J. F. Jurgens, *J. Am. Chem. Soc.* **1948**, 70, 1919-1920

20 G. Wegner, V. Buchholz, L. Ödberg, S. Stemme, *Adv. Mater.* **1996**, 8, 399-402

21 I. R. Peterson, *J. Phys. D: Appl. Phys.* **1990**, 29, 379-395

22 E. Kontturi, P. C. Thüne, J. W. Niemantsverdriet, *Polymer* **2003**, 44, 3621-3625

23 E. Kontturi, P. C. Thüne, J. W. Niemantsverdriet, *Langmuir* **2003**, 19, 5735-5741

24 S. Rohm, U. Hirn, C. Ganser, C. Teichert, R. Schennach, *Cellulose* **2014**, 21, 237-249

25 M. Tanaka, A. P. Wong, F. Rehfeldt, M. Tutus, S. Kaufmann, *J. Am. Chem. Soc.* **2004**, 126, 3257-3260

26 R. Kargl, T. Mohan, S. Köstler, S. Spirk, A. Doliška, K. Stana-Kleinschek, V. Ribitsch, *Adv. Funct. Mater.* **2013**, 23, 308-315

27 A. Petritz, A. Wolfberger, A. Fian, M. Irimia-Vladu, A. Haase, H. Gold, T. Rothländer, T. Griesser, B. Stadlober, *Appl. Phys. Lett.* **2013**, 103, 153303

28 M. Bračič, T. Mohan, R. Kargl, T. Griesser, S. Hribernik, S. Köstler, K. Stana-Kleinschek, L. Fras-Zemljič, *RSC Adv.* **2014**, 4, 11955

29 T. Mohan, R. Kargl, S. Köstler, A. Doliška, G. Findenig, V. Ribitsch, K. Stana-Kleinschek, *ACS Appl. Mater. Interfaces* **2012**, 4, 2743-2751

30 M. Tanaka, S. Kaufmann, J. Nissen, M. Hochrein, *Phys. Chem. Chem. Phys.* **2001**, 3, 4091-4095

31 S. Jung, B. Angerer, F. Löscher, S. Niehren, J. Winkle, S. Seeger, *ChemBioChem* **2006**, 7, 900-903

32 K. Ofir, Y. Berdichevsky, I. Benhar, R. Azriel-Rosenfeld, R. Lamed, Y. Barak, E. A. Bayer and E. Morag, *Proteomics* **2005**, 5, 1806-1814

33 S. R. Scheicher, K. Krammer, A. Fian, R. Kargl, V. Ribitsch, S. Köstler, *Per. Pol. Chem. Eng.* **2014**, 58, 61-67

34 S. Grilli, V. Vespini, P. Ferraro, *Langmuir* **2008**, 24, 13262-13265

35 D. C. Duffy, J. Cooper McDonald, O. J. A. Schueller, G. M. Whitesides, *Anal. Chem.* **1998**, 70, 4974-4984

36 J. H. Flynn, W. K. Wilson, W. L. Morrow, *Journal of Research of NIST* **1958**, 60, 229-233

37 A. Bos, A. S. Buchanan, *J. Polym. Sci. Polym. Chem. Ed.* **1973**, 11, 833-852

38 H. Ito, C. G. Willson, J. M. J. Frechet, *US. Patent* 4491628, **1985**

39 M. Shirai, M. Tsunooka, *Prog. Polym. Sci.* **1996**, 21, 1-45

40 K. Hosono, A. Kanazawa, H. Mori, T. Endo, *J. Appl. Polym. Sci.* **2008**, 109, 3157-3164

41 K. Hosono, A. Kanazawa, H. Mori, T. Endo, *Cellulose* **2007**, 14, 529-537

42 M. Shirai, M. Tsunooka, *Bull. Chem. Soc. Jpn.* **1998**, 71, 2483-2507

43 J. Gawroński, K. Gawrońska, P. Skowronek, A. Holmén, *J. Org. Chem.* **1999**, 64, 234-241

44 J.-P. Malval, F. Morlet-Savary, X. Allonas, J.-P. Fouassier, S. Suzuki, S. Takahara, T. Yamaoka, *Chem. Phys. Let.* **2007**, 443, 323-327

45 J.-P. Malval, S. Suzuki, F. Morlet-Savary, X. Allonas, J.-P. Fouassier, S. Takahara, T. Yamaoka, *J. Phys. Chem. A* **2008**, 112, 3879-3885

46 G. Pohlers, J. C. Scaiano, R. Sinta, R. Brainard, D. Pai, *Chem. Mater.* **1997**, 9, 1353-1361

47 G. Pohlers, J.C. Scaiano, R. Sinta, *Chem. Mater.* **1997**, 9, 3222-3230

48 G. Pohlers, J. C. Scaiano, E. Step, R. Sinta, *J. Am. Chem. Soc.* **1999**, 121, 6167-6175

49 J. L. Dektar, N. P. Hacker, *J. Org. Chem.* **1988**, 53, 1833-1835

50 J. L. Dektar, N. P. Hacker, *J. Photochem. Photobiol., A. Chem.* **1989**, 46, 233-238

51 J. L. Dektar, N. P. Hacker, *J. Am. Chem. Soc.* **1990**, 112, 6004-6015

52 N. P. Hacker, K. M. Welsh, *Macromolecules* **1991**, 24, 2137-2139

53 N. P. Hacker, J. L. Dektar, D. V. Leff, S. A. Macdonald, K. M. Welsh, *J. Photopolym. Sci. Technol.* **1991**, 4, 445-453

54 K. M. Welsh, J. L. Dektar, M. A. Garcia-Garibaya, N. P. Hacker, N. J. Turro, *J. Org. Chem.* **1992**, 57, 4179-4184

55 N. P. Hacker, D. C. Hofer, K. M. Welsh, *J. Photopolym. Sci. Technol.* **1992**, 5, 35-46

56 I. Horcas, R. Fernandez, J. M. Gomez-Rodriguez, J. Colchero, J. Gomez-Herrero, A. M. Baro, *Rev. Sci. Instrum.* **2007**, 78, 013705

57 A. Turbak, *TAPPI* **1984**, 67, 94-97

58 W. Schempp, T. Krause, U. Seifried, A. Koura, *Das Papier* **1984**, 38, 607-610

59 A. Koschella, D. Klemm, *Macromol. Symp.* **1997**, 120, 115-125

60 U. Henniges, P. Vejdovszky, M. Siller, M.-J. Jeong, T. Rosenau, A. Potthast, *Curr. Chromatogr.* **2014**, 1, 52-68

61 T. Heinze, R. Dicke, A. Koschella, A. H. Kull, E.-A. Klohr, W. Koch, *Macromol. Chem. Phys.* **2000**, 201, 627-631

62 M. Kostag, T. Liebert, O. A. El Seoud, T. Heinze, *Macromol. Rapid Commun.* **2013**, 34, 1580-1584

63 R. P. Swatloski, S. K. Spear, J. D. Holbrey, R. D. Rogers, *J. Am. Chem. Soc.* **2002**, 124, 4974-4975

64 W. Mormann, M. Wezstein, *Macromol. Biosci.* **2009**, 9, 369-375

65 K. Petzold, A. Koschella, D. Klemm, B. Heublein, *Cellulose* **2003**, 10, 251-269

66 R. H. Marchessault, C. Y. Liang, *J. Polym. Sci.* **1960**, 43, 71-84

67 H. G. Higgins, C. M. Stewart, K. J. Harrington, *J. Polym. Sci.* **1961**, 51, 59-84

68 G. Socrates, *Infrared and Raman Characteristic Group Frequencie: Tables and Charts*, 3rd Edition, John Wiley and Sons Ltd, Chichester, **2001**

69 U. Falk, W. Hickel, D. Lupo, U. Scheunemann, *US. Patent* 5402262, **1995**

70 D. Breitwieser, M. Kriechbaum, H. M. A. Ehmann, U. Monkowius, S. Coseri, L. Sacarescu, S. Spirk, *Carbohydrate Polymers* **2015**, 116, 261-266

71 M. L. Nelson, R. T. O'Connor, *J. Appl. Polym. Sci.* **1964**, 8, 1311-1324

72 K. Stana-Kleinschek, S. Spirk, T. Griesser, W. Kern, R. Kargl, V. Ribitsch, *Eur. Pat. Appl.* 2784586, **2014**

73 T. Mohan, S. Spirk, R. Kargl, A. Doliška, H. M. A. Ehmann, S. Köstler, V. Ribitsch, K. Stana-Kleinschek, *Colloids and Surfaces A: Physicochem. Eng. Aspects* **2012**, 400, 67-72

74 E. Kontturi, A. Lankinen, *J. Am. Chem. Soc.* **2010**, 132, 3678-3679

75 T. Mohan, R. Kargl, A. Doliška, A. Vesel, S. Köstler, V. Ribitsch, K. Stana-Kleinschek, *Journal of Colloid and Interface Science* **2011**, 358, 604-610

76 A. Wolfberger, A. Petritz, A. Fian, J. Herka, V. Schmidt, B. Stadlober, R. Kargl, S. Spirk, T. Griesser, *Cellulose* **2015**, 22, 717-727